10 Hydrogen Storage

Fuelled by concerns of air pollution, energy security and climate change, the notion of a 'hydrogen economy' is moving beyond the realm of scientists and engineers and into the lexicon of political and business leaders.[1] The concept of sustainable development has evolved into a guiding principle for a livable future world where human needs are met while keeping the balance with nature. Driving the global energy system into a sustainable path is progressively becoming a major concern and prime objective. Hydrogen has an outstanding potential for being a key factor in driving the energy sector to a sustainable trajectory. Hydrogen is the power source of our sun. More than 30% of the mass of the sun is atomic hydrogen. Hydrogen offers the long-term potential for an energy system that produces heat and zero emissions and is based on domestically available resources. It is sustainable since it can be produced not only from fossil fuels such as coal and natural gas, but also from solar, wind, thermal and hydroelectric power, biomass or municipal solid wastes, with no consumption of non-renewable energy resources and not much pollution of any kind. Interest in hydrogen, the simplest and most abundant element in the universe, is also rising due to technical advances in fuel cells—the potential successors to batteries in portable electronics, power plants and the internal combustion engine. It is necessary that we state again that hydrogen is not a source of energy, but an energy carrier.

Though there are quite a number of primary energy sources available, such as thermonuclear, nuclear, solar, wind, hydro, geothermal, and so on, in contrast to the fossil fuels, in most cases, these primary energy sources cannot be used directly (that is, used as fuels for transportation), and thus they must be converted into fuels, that is to say, an energy carrier is needed. Among the many choices, hydrogen is one of the best candidates. Hydrogen is an ideal fuel and versatile energy carrier, and its advantages include the following aspects:

- Available
- Easy to produce
- Renewable
- Convenient fuel for transportation
- Versatile, converts easily to other energy forms at the user end
- High utilization efficiency
- Environmentally compatible (zero- or low-emission)

Though energy can be stored in different forms, chemical and electric energy can be transmitted easily since they both involve electronic coulomb interaction. Chemical energy is based on the energy of unpaired outer valence electrons waiting to be stabilized by electrons from other atoms. The hydrogen atom is the most attractive because its electron (for charge neutrality) is accompanied by only one proton. Hydrogen thus has the best ratio of valence electrons to protons (and neutrons)

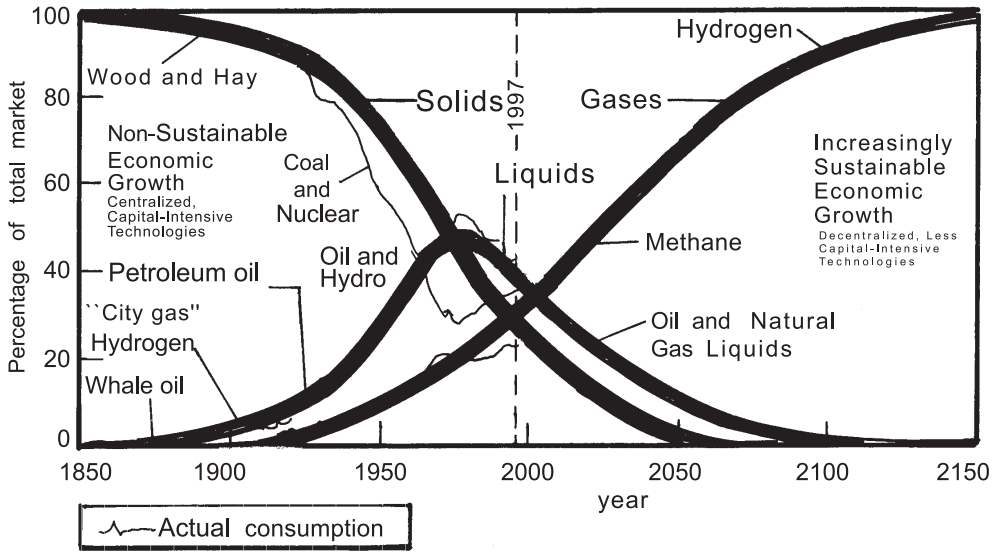

Figure 10.1 Global energy systems transition, 1850–2150[2]

of all the elements in the periodic table and the energy gain per electron is very high. The chemical energy per mass of hydrogen (142 MJ kg^{-1}) is at least three times larger than that of other chemical fuels. For example, the equivalent value for liquid hydrocarbon is 47 MJ kg^{-1}.

In the global energy scenario, the reality of an eventual transition to hydrogen becomes more evident when one takes an atomic view of energy history. Since the mid-19th century, the world has been slowly shifting from one form of energy to another—from solids to liquids to gases, as Robert Hefner of the GHK Company has illustrated in Fig. 10.1.[2]

Until the middle of the 19th century, reliance on wood for energy was common in most settled parts of the world. But in Great Britain, where population density and energy use were growing rapidly, wood began to lose out to coal, an energy source that was as abundant as wood but more concentrated, and not as bulky or awkward to transport. Coal remained king of the energy world for the remainder of the 19th century and well into the 20th century. But by 1900, the advantages of an energy system based on fluids, rather than solids, began to emerge as the transportation system started to shift away from railroads and towards automobiles. This shift created problems for coal, with its weight and volume, and at the same time it generated opportunities for oil, which featured a higher energy density and an ability to flow through pipelines and into tanks. By the mid-20th century, oil had become the world's leading energy source.

But dominant as oil is, the liquid now faces an up-and-coming challenger—gas. Despite improvements from wellhead to petrol pump, the distribution of oil is rather cumbersome. Natural gas, in addition to being cleaner and lighter and burning more efficiently, can be distributed through a network of pipes that is less conspicuous, more efficient, and more extensive than the one used for oil. As far as use is concerned, natural gas is now the fastest-growing fossil fuel, the fuel of choice for electricity, and the second-leading energy source, overtaking coal in 1999.

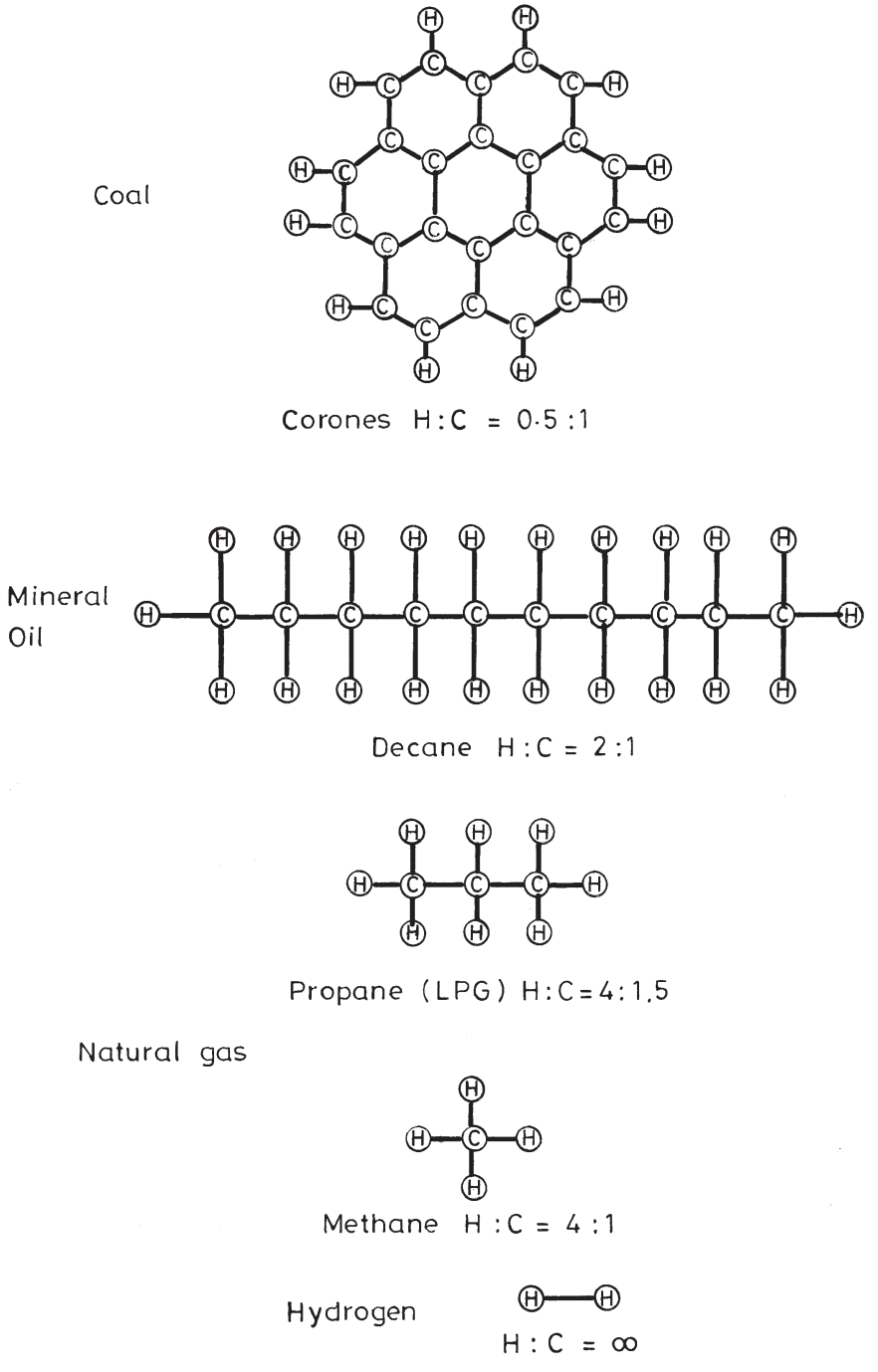

Figure 10.2 The atomic hydrogen–carbon ratio

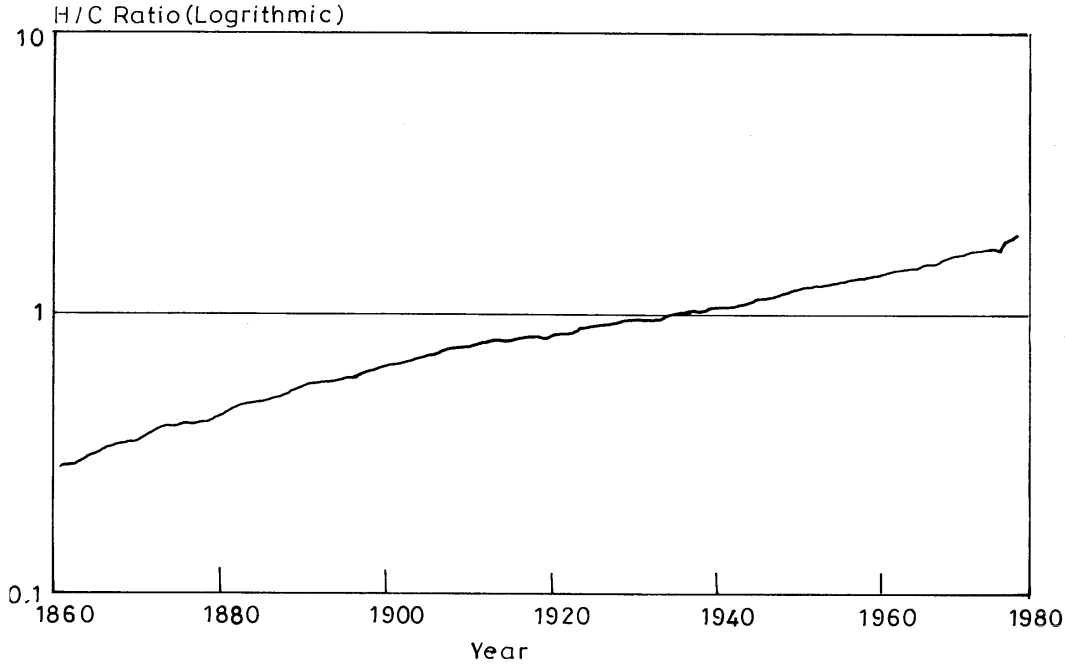

Figure 10.3 Hydrogen-to-carbon ratio, world energy mix, 1860–1990

The move from solid fuels to liquid fuels to gas fuels involves another sort of transition: the less visible process of 'decarbonization'. From wood to coal to oil to natural gas, the ratio of hydrogen (H) to carbon (C) in the molecule of each successive source has increased. Roughly speaking, the ratio is between 1–3 and 1–10 for wood; 1–2 for coal; 2–1 for oil; and 4–1 for natural gas (Fig. 10.2). Between 1860 and 1990, the hydrogen-to-carbon ratio rose six-fold (Fig. 10.3).

The next logical fuel in this progression is hydrogen, the lightest and most abundant element in the universe and the power source of our Sun. Found on Earth in water, life forms and hydrocarbon fuels, hydrogen is already established in space programmes and industrial applications. The emergence of hydrogen as a major energy carrier could initially build on the existing natural gas network for its distribution, with the hydrogen derived at first from natural gas to run high-efficiency fuel cells. Eventually, hydrogen will likely use its own full-fledged network, created by splitting water into hydrogen and oxygen using electricity from solar, wind, and other forms of renewable energy. The production of hydrogen from virtually limitless stores of renewable sources will free the energy system from carbon.

Hydrogen has long been recognized as a fuel having some unique and highly desirable properties, for application as a fuel in engines.[3] It is the only fuel that can be produced entirely from the plentiful renewable resource water, albeit through the expenditure of relatively much energy. Its combustion in oxygen uniquely produces only water, but in air it also produces some oxides of nitrogen. These features make hydrogen an excellent fuel. The viability of hydrogen as a fuel in

general, and in engine applications in particular, is critically dependent on the effective, economic and satisfactory solution of a number of key limiting problems. These limitations that hinder its widespread application as an engine fuel are primarily related to its *production, storage, portability, transportation* and *purity*. These limitations can be considered to be far more serious than those facing the current and future applications of other fuels, including natural gas.

10.1 Hydrogen Production

The main feature of hydrogen as a fuel is that it does not occur in its free state naturally. Though hydrogen is the most abundant element on earth, less than 1% is present as molecular hydrogen gas H_2. The gas must be manufactured from a wide variety of possible sources which require much energy and capital resources.[4] Direct thermal dissociation of water requires temperatures higher than 2,000 °C (> 900 °C with Pt/Ru catalysts). Hydrogen can be produced from fossil fuels such as natural gas, oil and coal, mainly via their reforming with steam or through partial oxidation. These approaches are often through the application of suitable catalysts; but non-catalytic approaches are also commonly used. The hydrogen produced through these measures will be in association with a wide range of products, including carbon-bearing compounds such as carbon monoxide and carbon dioxide. Such fuel mixtures of widely varying composition are usually processed further to increase the purity of the hydrogen produced, whether for applications in the chemical and petrochemical industries or for combustion in conventional power and heating devices. However, for the increasingly important application of hydrogen in fuel cells, hydrogen of ultra-high purity is required, while the hydrogen produced by the above methods is often of unacceptable quality.[5]

Hydrogen can be produced in sufficiently high purity for fuel cell applications through the electrolysis of water with thermal efficiency ranging from 60%–75%.[6] Much of the electrical power required for hydrogen production is often supplied by hydroelectric sources. However, depending on the availability and cost, the electric energy used may be generated via nuclear power or thermal power stations burning fossil fuels. However, the overall efficiency of hydrogen production from fossil fuels on energy basis will be lower than 35%.[7] Also, in principle, electric power can be produced occasionally in very limited quantities from other energy sources such as those derived from the sun, wind, sea waves and tides. At present, the prospects of producing hydrogen in significant quantities via biological processes, chemical reactive cycles and the oxidation of metals remain remote.

The cost of hydrogen depends on how one makes it. Today, the most inexpensive production method is the steam reformation of natural gas (heating methane under high pressure with a catalyst in a steam atmosphere), which has been able to produce hydrogen for as low as US $0.96 for the same energy as a gallon of petrol. The price of hydrogen made by this method does rise with the price of natural gas, however. Other methods, such as electrolysis of water (H_2O) into hydrogen and oxygen (electrolysis), chemical reactions, and biomass digestion, vary in their prices. Typically, the cost of hydrogen production ranges from about only twice to more than ten times higher than the cost of production of pipeline natural gas on energy equivalent basis. With so many ways to produce hydrogen, there will definitely be at least one method that will be more economical than petroleum, as the supplies of petroleum are outpaced by demand.

10.2 Some Relevant Properties

Some of the key overall properties of hydrogen that are relevant to its employment as an engine fuel are listed in Table 10.1. These are compared to the corresponding values of methane, the other promising gaseous fuel for engine applications, and those of iso octane vapour, representing petrol.[8]

It is evident that hydrogen is a remarkably light gaseous fuel that requires on volume basis the least amount of air for stoichiometric combustion (2.39 as against 59.6 for iso-octane); while on mass basis it requires the highest relative mass of air. Its combustion is also associated with a substantial molar contraction of around 15%. Its heating value on mass basis is the highest; but on volume basis it is the lowest. Also, since its product of combustion in air is only water, there is a significant difference between its higher and lower heating values. However, its energy release by combustion per unit mass of stoichiometric mixture is one of the highest.

Hydrogen has some remarkably high values of the key properties for transport processes, such as kinematic viscosity, thermal conductivity and diffusion coefficient, in comparison to those of

Table 10.1 Some comparative properties of hydrogen, methane and isooctane

Property	Hydrogen	Methane	Petrol
Density at 1 atm and 300 K (kg)/m^3	0.082	0.717	5.11
Stoichiometric composition in air (% by volume)	29.53	9.48	1.65
Stoichiometric fuel/air mass ratio	0.029	0.058	0.0664
No. of moles after conbustion to before	0.85	1.00	1.058
Heating values			
Highest Heating Value (HVH) (MJ/kg)	141.7	52.68	48.29
Lowest Heating Value (HVH) (MJ/kg)	119.7	46.72	44.79
Highest Heating Value (HVH) (MJ/m^3)	12.10	37.71	233.29
Lowest Heating Value (HVH) (MJ/m^3)	10.22	33.95	216.38
Combustion energy per kg of stoichiometric mixt. (MJ)	3.37	2.56	2.79
Kinematic viscosity at 300 K (mm^2/s)	110	17.2	1.18
Thermal conductivity at 300 K (mW/mK)	182.0	34.0	11.2
Diffusion coefficient into air NTP (cm^2/s)	0.61	0.189	0.05

Table 10.2 Some comparative combustion properties of hydrogen, methane and petrol

Property	Hydrogen	Methane	Petrol
Flammabiliity (% by volume)	4–75	5.3–15.0	1.2–6.0
Minimum ignition energy (mJ)	0.02	0.28	0.25
Laminar flame speed at NTP (m/s)	1.90	0.38	0.37–0.43
Adiabatic flame temp (K)	2318	2190	~ 2,470
Autoignition temperature (K)	858	813	~ 500–750
Quenchning gap at NTP (mm)	0.64	2.03	

the other two fuels. Such differences together with its extremely low density and low luminosity, help to give hydrogen its unique diffusive and heat transfer characteristics.

Some combustion properties that have much influence on the potential behaviour of hydrogen as a fuel in general, and for engine applications in particular, are given in Table 10.2. The corresponding values for the other representative fuels, methane and commercial petrol, are also shown for comparison. It can be seen that hydrogen has a remarkably wide flammable mixture range in air to permit extremely lean or rich mixtures to support combustion. It requires also a remarkably low minimum amount of energy to effect ignition with extremely fast resulting flames in comparison to those of mixtures of methane or even iso-octane with air. However, the values of its spontaneous ignition temperatures are quite similar to those of the other two fuels and the values of its maximum adiabatic combustion temperature in air are only a little higher.

The kinetics of the combustion of hydrogen in air is well understood at present and its oxidation reaction rates and the associated temporal variation of the concentrations of the reactive species can be predicted well. Mainly relatively fast and nearly thermally neutral, branching chain reactions are involved. On the other hand, oxidation of hydrocarbon fuels normally involve thermally significant chain reactions that contain relatively slower endothermic reaction steps that are associated with fuel breakdown. These differences, together with those in the thermodynamic and transport properties of hydrogen, contribute in a big way to the substantially different combustion characteristics of hydrogen from those of other common fuels.

10.3 Hydrogen as an Engine Fuel

10.3.1 Positive features of hydrogen for engine applications

There are a number of unique features associated with hydrogen that make it remarkably well suited in principle, to engine applications.[9] Some of the most notable features are the following:

Hydrogen, in over wide temperature and pressure ranges, has very high flame propagation rates within the engine cylinder in comparison to other fuels. These rates remain sufficiently high even for very lean mixtures that are well away from the stoichiometric mixture region. The associated energy release is also so fast that the combustion duration, as shown typically in Fig. 10.4, tends

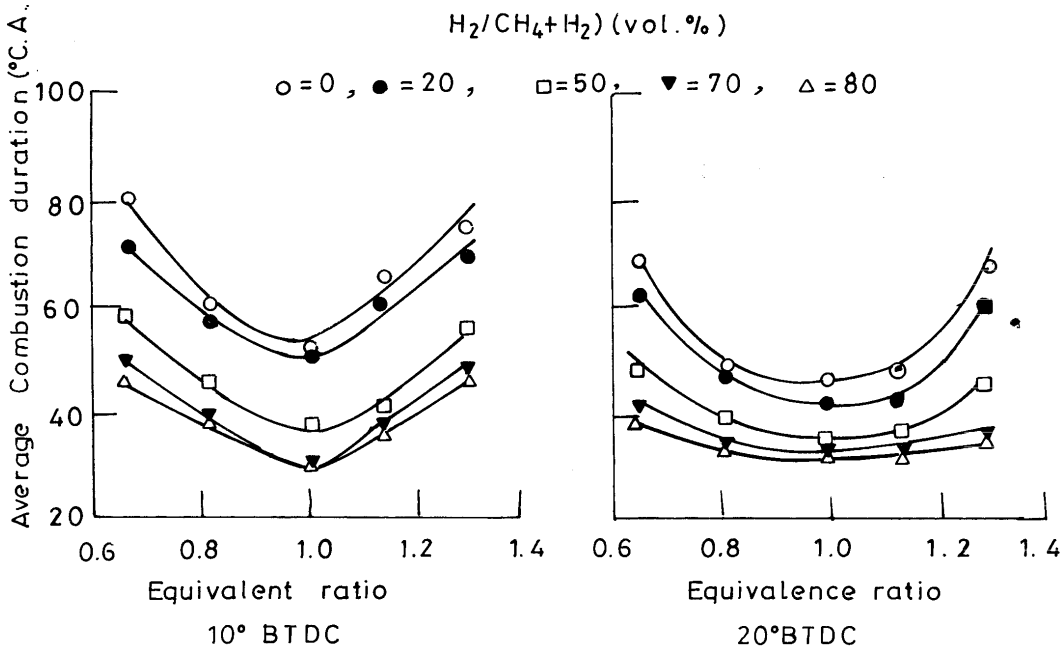

Figure 10.4 Typical variations in the length of the combustion period in degrees with equivalence ratio for a range of H_2–CH_4 mixtures for two spark timings at a compression ratio of 8.5:1 and 900 rev/min[10]

to be short and contributes towards producing high-power output efficiencies and high rates of pressure rise following spark ignition.[10]

The lean operational limit mixture in a spark ignition engine when fuelled with hydrogen is very much lower than those for other common fuels, as shown typically in Fig. 10.5 for a range of compression ratios. This permits stable lean mixture operation and control in hydrogen fuelled engines.[11]

The operation on lean mixtures, in combination with the fast combustion energy release rates around top dead centre (TDC) associated with the very rapid burning of hydrogen–air mixtures results in high-output efficiency values. Of course, such lean mixture operation leads simultaneously to a lower power output for any engine size, as shown typically in Fig. 10.6.

One of the most important features of hydrogen engine operation is that it is associated with less undesirable exhaust emissions than for operation on other fuels. As far as emissions are concerned, there are no unburnt hydrocarbons, carbon monoxide, carbon dioxide, oxides of sulphur, smoke or particulates.[12] The contribution of lubricating oil to such emissions in well-maintained engines tends to be rather negligible. Only oxides of nitrogen and water vapour are the main products of the combustion emitted. Also, with lean operations the level of NO_x tends to be significantly smaller than those encountered with operation on other fuels.[13]

The fast burning characteristics of hydrogen permit satisfactory high-speed engine operation.[14] This would allow an increase in power output with a reduced penalty for lean mixture operation.

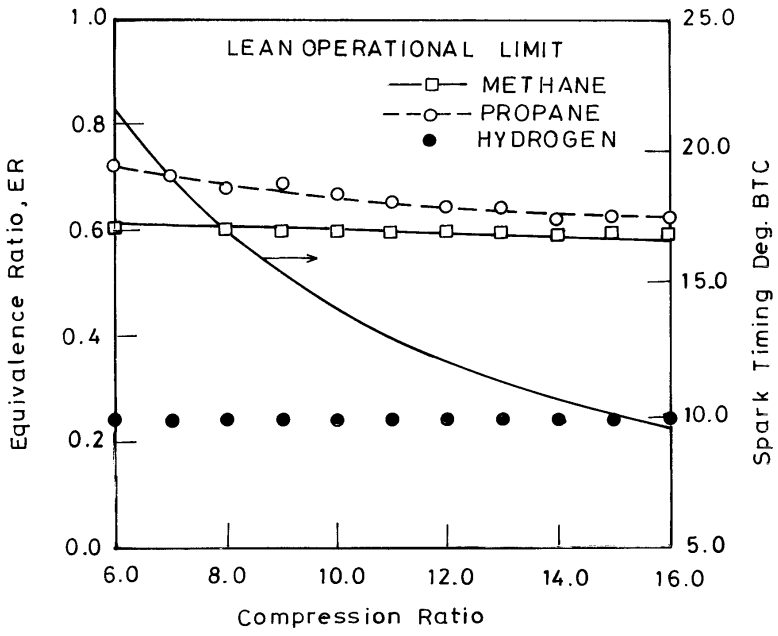

Figure 10.5 Variations of the lean operational limits with changes in compression ratio for different gaseous fuels at 900 rev/min[11]

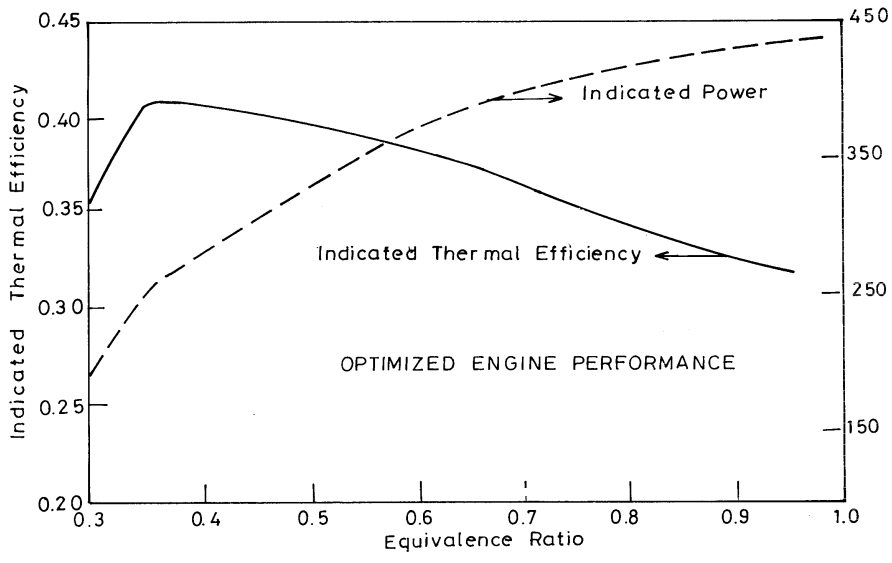

Figure 10.6 Typical variations in the indicated power output and efficiency with leaning of equivalence ratio for hydrogen operation using optimum spark timing[9]

Also, the extremely low boiling temperature of hydrogen leads to fewer problems encountered with cold weather operation.

Varying the spark timing in hydrogen engine operation is an unusually effective means for improving engine performance and avoiding the incidence of knock (Fig. 10.7). Also, the heat transfer characteristics of hydrogen combustion in engines are significantly different from those in engines operating on other fuels. The radiative component of heat transfer tends to be small yet the convective component can be higher, especially for lean mixture operation.

The sensitivity of the oxidation reactions of hydrogen to catalytic action with proper control can be made to serve positively towards enhancing engine performance.

Some other positive features of hydrogen for engine applications

In addition to the above unique features associated almost exclusively with hydrogen, a number of others can be cited in support of hydrogen applications in engines. The following is a listing of some of the main features:

- Less cyclic variations are encountered with hydrogen than with other fuels, even for very lean mixture operation. This leads to a reduction in emissions, improved efficiency, and quieter and smoother operation.

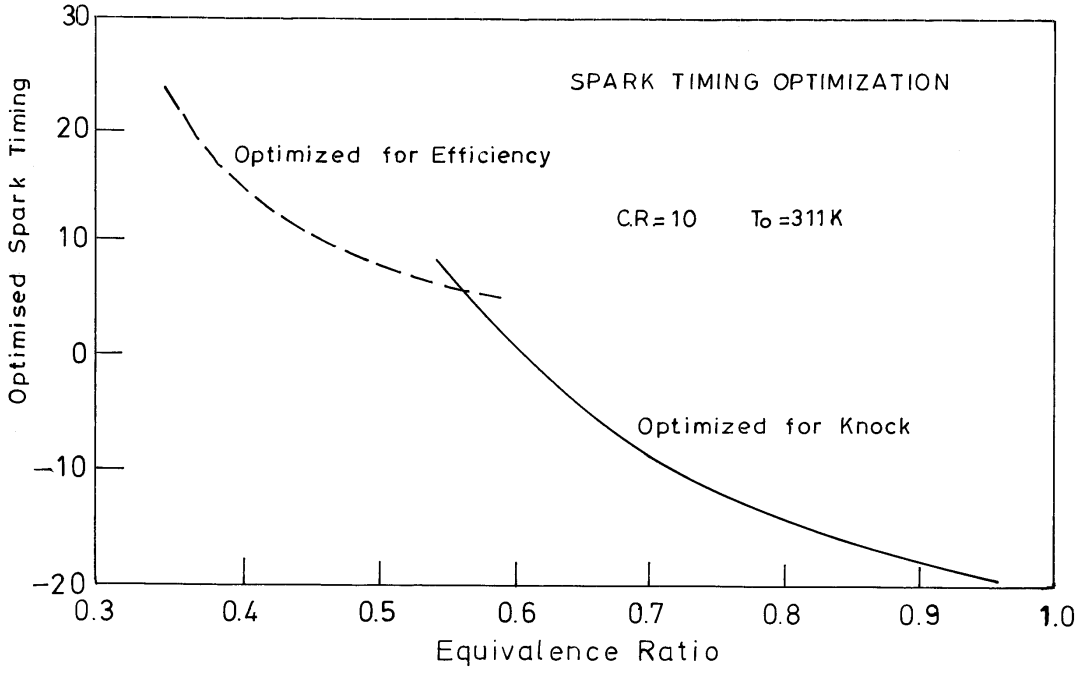

Figure 10.7 Typical variations in spark timing for optimum efficiency and avoidance of knock for lean mixture operation with hydrogen[9]

- Hydrogen can have a high effective octane number, mainly because of its high burning rates and its slow pre-ignition reactivity.
- Hydrogen has been shown to be an excellent additive in relatively small concentrations, to some common fuels such as methane.[10]
- Its gaseous state permits excellent cold starting and engine operation.
- Hydrogen engines are more amenable to high-speed operation mainly due to the associated fast burning rates.
- Less spark advance is usually needed, which contributes to better efficiencies and improved power output as the bulk of the heat release by combustion can be completed just after the TDC region.
- Hydrogen engine operation can be associated with less heat loss than with other fuels.
- Moderately high compression ratio operation is possible with lean mixtures of hydrogen in air, which permits higher efficiencies and increased power output.
- Hydrogen engines are very suitable for co-generation applications since the energy transfer due to condensing some water vapour can add up significantly to the thermal load output and the corresponding energy efficiency.
- Hydrogen, unlike most other commercial fuels, is a pure fuel of well-known properties and characteristics, which permits continued and better op timization of engine performance.
- The reaction rates of hydrogen are sensitive to the presence of a wide range of catalysts. This feature helps to improve its combustion and the treatment of its exhaust emissions.
- The thermodynamic and heat transfer characteristics of hydrogen tend to produce high compression temperatures that contribute to improvements in engine efficiency and lean mixture operation.
- The high burning rates of hydrogen make the performance of hydrogen fuelled engine less sensitive to changes in the shape of the combustion chamber, level of turbulence and the intake charge swirling effect.
- Hydrogen can better tolerate the presence of diluents. This would allow a better exploitation of low heating value fuel mixtures.
- Hydrogen can be employed quite effectively with oxygen-enriched air such as that resulting from the electrolysis of water.
- Unlike most fuel cells the spark ignition engine is quite tolerant to not-so-pure fuel.
  The gas is highly diffusive and buoyant, which makes fuel leaks disperse quickly, reducing the hazards of fire and explosion associated with hydrogen engine operation.

10.3.2 Limitations associated with hydrogen engine applications

Much of the information reported in the open literature on the performance of engines with hydrogen as a fuel tends to highlight the positive features of hydrogen while de-emphasizing or even ignoring the many limitations associated with such fields of application. There is a need to focus equally well on these and suggest means for overcoming some of their negative aspects. Accordingly, the following is a listing of some features associated with hydrogen as an engine fuel that may be considered as requiring some remedial action:

- Hydrogen as a compressed gas at 200 atmospheres and atmospheric temperature has merely around 5% of the energy of petrol of the same volume. This is a major shortcoming, particularly for transport applications.
- Engines fuelled with hydrogen suffer from reduced power output, due mainly to the very low heating value of hydrogen on volume basis and resorting to lean mixture operation.
- The mass of the intake air is reduced for any engine size because of the relatively high stoichiometric hydrogen to air ratio.
- There are serious potential operational problems associated with the uncontrolled pre-ignition and backfiring into the intake manifold of hydrogen engines.[15]
- Hydrogen engines are prone to produce excessively high cylinder pressure and are prone to the onset of knock. The equivalent octane number of hydrogen is rather low in comparison to common petrol and methane.[16]
- The high burning rates of hydrogen produce high pressures and temperatures during combustion in engines when operating near stoichiometric mixtures. This may lead to high exhaust emissions of oxides of nitrogen.
- There are serious limitations to the application of cold exhaust gas recirculation for exhaust emissions control.
- Hydrogen engines may display some serious limitations to effective turbo charging.
- There is always some potential for increased safety problems with hydrogen operation.[17]
- Hydrogen engine operation may be associated with increased noise and vibrations due mainly to the high rate of pressure rise resulting from fast burning.
- Great care is needed to avoid material compatibility problems with hydrogen applications in engines.
- In certain applications, such as in very cold climates, the exhaust emission of steam can be an undesirable feature, leading to poor visibility and increased icing problems.
- The sensitivity of hydrogen–air mixtures to catalytic action can be occasionally considered undesirable as it may contribute to reduced safety and poorer control of the combustion process.
- Hydrogen requires a very low ignition energy, which leads to uncontrolled pre-ignition problems.
- There is an increased potential for undesirable corrosion and lubricating oil contamination due to exhaust water vapour condensation.
- There can be an increased potential for operational durability problems with lubricants.
- Heat transfer losses can be high, yet under some conditions they can be quite low.
- A hydrogen engine needs to be some 40%–60% larger in size than a petrol engine for the same power output. This could lead to some reduction in engine speed, increased mechanical and motoring losses and reduced tolerance to knocking. Also, some engine design modifications are needed.

A number of possible changes essential to the design and operational features of a hydrogen fuelled spark ignition (SI) engine are suggested by Karim[9] to effect the full potential of hydrogen in engine applications.

Significant news has come from vehicle corporations such as Daimler-Chrysler, Ford, General Motors, Toyota, Honda, and others, that the development of proton-exchange membrane fuel cell (PEMFC) powered electric vehicles has been making great progress. Recently, the Daimler Chrysler Corporation. announced that it would be the first automaker worldwide to offer fuel cell vehicles on the market during the next several years.[18] However, several barriers have to be overcome before hydrogen electric vehicles can be put into large-scale practical utilization. One of the significant challenges is the lack of a safe and efficient on-board storage technology, which may dramatically influence the vehicle's cost, range, performance and fuel economy, as well as shape the scale, investment requirements, energy use and potential emissions of a hydrogen-refuelling infrastructure. Hydrogen is used as a fuel in vehicles in three main ways: in a nickel-hydride battery, in which hydrogen is in a combined state as a metal hydride; directly in a spark-ignition engine powered car; and as fuel in a fuel cell. In the last case, hydrogen can be converted to electricity with emission of only water, with high efficiency because the process is not subject to the limitations of the Carnot Cycle. Thus, true zero-emission vehicles can probably be realized.

The problem of using hydrogen as a fuel for transportation is that there is no suitable means of storage.

10.4 Methods of Hydrogen Storage

On-board storage is the critical issue with regard to hydrogen's utility as an energy carrier for any mode of transportation on land, sea or air. There are basically five practical options for the storage: (1) as gas at normal to medium pressure either in underground cavities and voids such as dried up oil and gas wells, aquifers and salt caverns or in telescoping water-sealed gas-holders, (2) as compressed gas in heavy steel containers, (3) as cryogenic liquid in insulated containers, (4) in the form of chemical compounds such as hydrocarbons, methanol and ammonia, from which hydrogen can be produced by thermal decomposition, (5) as decomposable metal hydrides and (6) in some other form. We shall now examine each of the above storage options one by one.

Hydrogen storage is a materials science challenge because, for all six storage methods currently being investigated, materials with either a strong interaction with hydrogen or without any reaction are needed. The goal is to pack hydrogen as close as possible, that is, to reach the highest volumetric density by using as little additional material as possible. Hydrogen storage implies the reduction of an enormous volume of hydrogen gas. At ambient temperature and atmospheric pressure, 1 kg of the gas has a volume of 11 m^3. To increase hydrogen density, work must be applied either to compress the gas, with the temperature decreased below the critical temperature, or to reduce repulsion by the interaction of hydrogen with another material.

The second important criterion for a hydrogen storage system is the reversibility of uptake and release. Materials that interact with hydrogen, therefore, as well as inert materials, are important. The reversibility criterion excludes all covalent hydrogen–carbon compounds because hydrogen is only released if it is heated to temperatures above 800 °C, or if the carbon is oxidized. Six methods of reversible hydrogen storage with high volumetric and gravimetric density are known today, as listed in Table 10.3. We shall discuss various hydrogen storage methods and illustrate their advantages and material challenges.

Table 10.3 The six basic hydrogen storage methods and phenomena. The gravimetric density ρ_m, the volumetric density ρ_v, the working temperature T, and pressure p are listed. RT stands for room temperature (25 °C)

Storage method	ρ_m [mass%]	ρ_m [kg H_2 m^3]	T[°C]	P [bar]	Phenomena and Remarks
High pressure gas cylinders	13	< 40	RT	800	Compressed gas (molecular H_2) in light weight composite cylindres (tensile strength of the material is 2,000 MPa)
Liquid hydrogen in cryogenic tanks	Size dependent	70.8	−252	1	Liquid H_2 (molecular H_2) continous loss of a few % per day of hydrogen at RT
Adsorbed hydrogen	∼ 2	20	−80	100	Physisorption (molecular H_2) on materials, example, carbon with a very large specific surface area, fully reversible
Adsorbed on interstitial	∼ 2	150	RT	1	Hydrogen (atomic hydrogen) intercalation in host sites in a host metal, metals, metallic hydrides working at RT are fully reversible
Complex compounds	< 18	150	> 100	1	Complex compounds ($[AlH_4^-]$ or $[BH_4]^-$), desorption at elevated temperatures, adsorption at high pressures
Metals and complexes together with water	< 40	> 50	RT	1	Chemical oxidation of metals with water and liberation of hydrogen, not directly reversible

10.4.1 Storing hydrogen as a gas

Three isotopes of hydrogen are known: hydrogen or protium (H), deuterium (D), and the unstable tritium (T). These isotopes of hydrogen form covalent molecules H_2, D_2, and T_2, respectively, because of the single electron in the atom. Hydrogen has an ambivalent behaviour towards other

elements, occurring as an anion (H^-) or cation (H^+) in ionic compounds; forming covalent bonds, example, with carbon; or even behaving like a metal to form alloys or intermetallic compounds at ambient temperature.

The phase diagram of the hydrogen molecule H_2 is shown in Fig. 10.8.[19] At low temperatures, hydrogen is a solid with a density of 70.6 kg m^{-3} at −262 °C, and a gas at higher temperatures with a density of 0.089886 kg m^{-3} at 0 °C and a pressure of 1 bar. Hydrogen is a liquid in a small zone between the triple and critical points with a density of 70.8 kg m^{-3} at −253 °C. At ambient temperature (298.15 K), hydrogen gas is described by the Van der Waals equation:

$$P(V) = nRT/(V - nb) - a(n^2/V^2) \tag{10.1}$$

where P is the gas pressure, V the volume, T the absolute temperature, n the number of moles, R the gas constant, a the dipole interaction or repulsion constant, and b the volume occupied by the hydrogen molecules.[20] The strong repulsive interaction between hydrogen is responsible for the low critical temperature ($T_c = 33$ K) of the gas.

10.4.2 High pressure gas cylinders

The most common storage system is high pressure gas cylinders, which are operated at a maximum pressure of 20 MPa. The wall thickness of a cylinder capped with two hemispheres is given by the following equation:

$$(d_w/d_o) = \Delta p/2\Sigma v + \Delta p \tag{10.2}$$

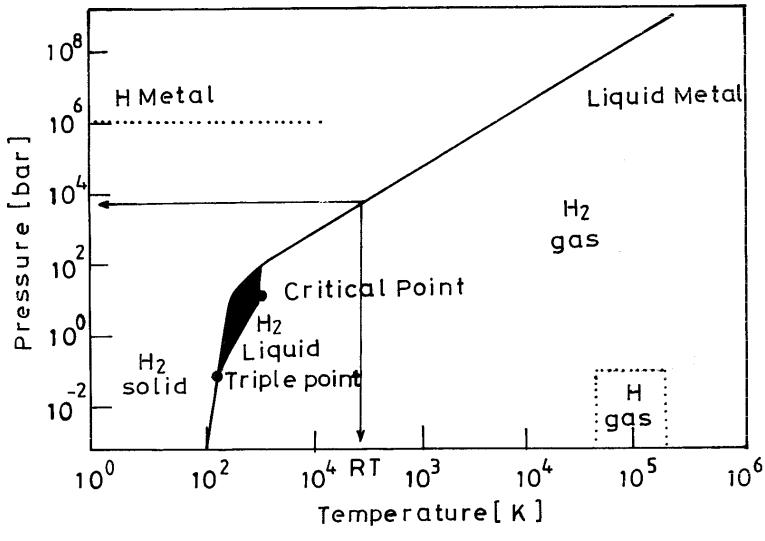

Figure 10.8 Primitive phase diagram for hydrogen.[19] Liquid hydrogen only exists between the solidus line and the line from the triple point at 21.2 K and the critical point at 32 K

where d_w is the wall thickness, d_o the outer diameter of the cylinder, Δp the over-pressure, and σ_V the tensile strength of the material. The tensile strength of materials varies from 50 MPa for Al to more than 1,100 MPa for high quality steel. Other materials like B have a tensile strength of up to 2,410 MPa and a density of only 2,370 kg m^{-3}. New lightweight composite cylinders have been developed that are able to withstand pressures upto 80 MPa, so that hydrogen can reach a volumetric density of 36 kg m^{-3}, approximately half as much as in its liquid form at normal boiling point. The ideal material for a high pressure cylinder has a very high tensile strength (not necessarily isotropic) and a low density, and does not react with hydrogen or allow hydrogen to diffuse into it. Most pressure cylinders to date have used austenitic stainless steel (for example, AISI 316 and 304 and AISI 316L and 304L above 300 °C to avoid carbon grain-boundary segregation[21]), or Cu or Al alloys, which are largely immune to hydrogen effects at ambient temperatures. Figure 10.9 shows the volumetric density of hydrogen inside the cylinder and the ratio of the wall thickness to the outer diameter of the pressure cylinder for stainless steel with a tensile strength of 460 MPa. The volumetric density increases with pressure and reaches a maximum above 1,000 bar, depending on the tensile strength of the material. However, the gravimetric density decreases with increasing pressure, and the maximum gravimetric density is found for zero over-pressure. Therefore, the increase in volumetric storage density is sacrificed with the reduction of the gravimetric density in pressurized gas systems.

The safety of pressurized cylinders is a concern, especially in highly populated regions. It is envisaged that future pressure vessels will consist of three layers: an inner polymer liner over-

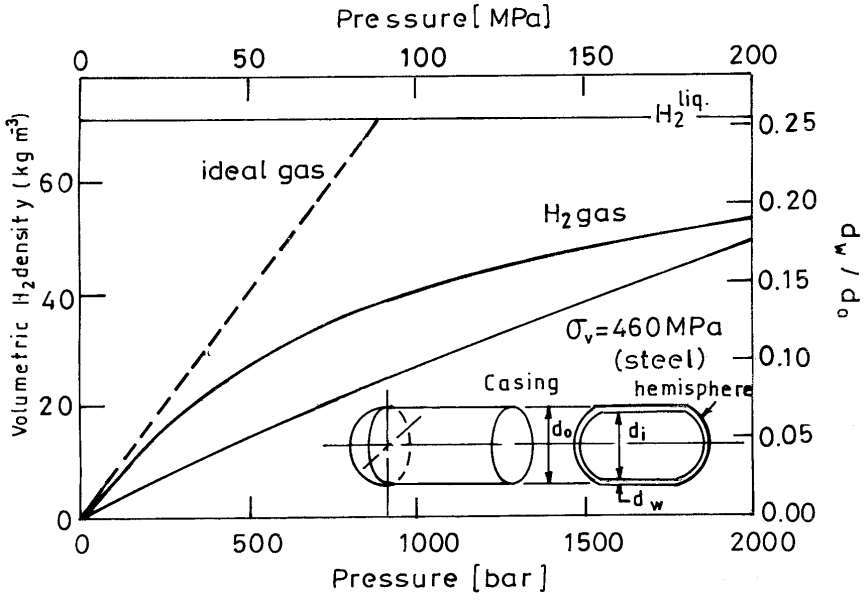

Figure 10.9 Volumetric density of compressed hydrogen gas as a function of gas pressure, including the ideal gas and liquid hydrogen. The ratio of the wall thickness to the outer diameter of the pressure cylinder is shown on the right hand side for steel with a tensile strength of 460 MPa. A schematic drawing of the pressure cylinder is shown as an inset

wrapped with a carbon-fiber composite (which is the stress-bearing component) and an outer layer of an aramid material capable of withstanding mechanical and corrosion damage. Industry has set itself a target of a 110 kg, 70 MPa cylinder with a gravimetric storage density of 6 mass% and a volumetric storage density of 30 kg m^{-3}.

Hydrogen can be compressed using standard, piston-type mechanical compressors. The theoretical work for the isothermal compression of hydrogen is given by the equation:

$$\Delta G = RT \text{ in } (P/P_o) \tag{10.3}$$

where R is the gas constant, T the absolute temperature, and p and p_0 the end pressure and the starting pressure, respectively. The error of the work calculated with (10.3) in the pressure range of 0.1–100 MPa is less than 6%. The isothermal compression of hydrogen from 0.1–80 MPa therefore consumes 2.21 kW h kg^{-1}. In a real process, the work consumption is significantly higher because compression is not isothermal. Compression ratios of greater than 20:1 are possible[22] with final pressures >100 MPa.

The relatively low hydrogen density together with the very high gas pressures in the system are important drawbacks of this technically simple and, on the laboratory scale, well established high pressure storage method.

10.4.3 Liquid hydrogen storage

Liquid hydrogen is stored in cryogenic tanks at 21.2 K at ambient pressure. Because of the low critical temperature of hydrogen (33 K), the liquid form can only be stored in open systems, as there is no liquid phase existent above the critical temperature. The pressure in a closed storage system at room temperature (RT) could increase to $\sim 10^4$ bar.

The simplest liquefaction cycle is the Joule–Thompson cycle (Linde cycle). The gas is first compressed and then cooled in a heat exchanger, before it passes through a throttle valve where it undergoes an isoenthalpic Joule–Thomson expansion, producing some liquid. The cooled gas is separated from the liquid and returned to the compressor via the heat exchanger.[23] The Joule–Thompson cycle works for gases, such as nitrogen, with an inversion temperature above RT. Hydrogen, however, warms upon expansion at RT. For hydrogen to cool upon expansion, its temperature must be below its inversion temperature of 202 K. Therefore, hydrogen is usually pre-cooled using liquid nitrogen (78 K), before the first expansion step occurs. The free enthalpy change[24] between gaseous hydrogen at 300 K and liquid hydrogen at 20 K is 11640 kJ kg^{-1}. The necessary theoretical energy (work) to liquefy hydrogen from RT is $W_{th} = 3.23$ kWh kg^{-1}; the technical work[25] is about 15.2 kWh kg^{-1}, almost half of the lower heating value of hydrogen combustion.

The boil-off rate of hydrogen from a liquid storage vessel, because of heat leaks, is a function of its size, shape and thermal insulation. Since boil-off losses as a result of heat leaks are proportional to the surface-to-volume ratio, the evaporation rate diminishes as the storage tank size increases. For double-walled, vacuum-insulated spherical dewars, boil-off losses are typically 0.4% per day for those with a storage volume of 50 m^3, 0.2% for 100 m^3 tanks, and 0.06% for 20,000 m^3 tanks.

The large amount of energy necessary for liquefaction and the continuous boil-off of hydrogen, limit the possible use of liquid hydrogen storage systems to applications where the cost of hydrogen is not an issue and the gas is consumed in a short time, example, air and space applications.

10.4.4 Storage via chemical reactions

Hydrogen can be generated by reacting metals and chemical compounds with water. A common experiment in which a piece of sodium floating on water produces hydrogen, demonstrates the process. The sodium transforms to NaOH in this reaction. The reaction is not directly reversible, but NaOH can be removed and reduced in a solar furnace back to metallic sodium. Two sodium atoms react with two H_2O molecules and produce one hydrogen molecule. The hydrogen molecule produces a H_2O molecule in combustion, which can be recycled to generate more hydrogen gas. However, the second H_2O molecule necessary for the oxidation of the two sodium atoms has to be added. Therefore, sodium gives rise to a gravimetric hydrogen density of 3 mass%. The same process carried out with lithium leads to a gravimetric hydrogen density of 6.3 mass%. The major challenge of this storage method is reversibility and control of the thermal reduction process in order to produce the metal in a solar furnace. The process has been successfully demonstrated with Zn.[26]

From all the above approaches, one can see that: (1) Underground storage is static and geospecific, whereas above-ground gas holders will occupy large land areas and carry the risks of uncontrollable fires and explosions. (2) High pressure gas storage involves the energy of compression (roughly 4 kcal/mole H_2 for compression to 140 atm tank pressure) and suffers from a heavy weight penalty and explosion risk. Being rather expensive, it can be justified only for the transportation of limited quantities of hydrogen for special applications. (3) Liquefaction and conversion to carbon and nitrogen compounds as hydrogen carriers require heavy plant investment and process infrastructures besides being highly energy intensive. Liquefaction of hydrogen consumes about 7 kcal per mole, which make it expensive. None of the above-mentioned methods (except perhaps underground storage and gas-holders) will permit direct 'recharging' of the storage medium with hydrogen in its normal gaseous state without intermediate conversion or processing.

Most automakers are considering either the high-pressure gaseous or cryogenic liquid hydrogen storage options for passenger vehicles. However, these two technologies are fraught with public perception on safety. Other issues also need to be addressed, including compression costs, safety, liquefaction costs, and dormancy.

The US Department of Energy (DOE) Hydrogen Plan has set a standard for this discussion by providing a commercially significant benchmark for the amount of reversible hydrogen adsorption. The benchmark requires a system-weight efficiency (the ratio of stored hydrogen weight to system weight) of 6.5 wt% hydrogen and a volumetric density of 62 kg H_2/m^3, since a vehicle powered by a fuel cell would require more than 3.1 kg of hydrogen for a 500 km range.[27] Figure 10.10 shows that neither of these storage options meets the long-term needs of automakers and barely those in the near-term.[27] For this reason, it is becoming increasingly accepted that the solid matrix method of hydrogen storage is the only option that has any hope of achieving the gravimetric and volumetric densities identified in Fig. 10.10 for the DOE goals.

Apart from engineering aspects, for the automobile industry to introduce hydrogen-powered fuel cell vehicles, they will need a safe, lightweight and compact means of on-board hydrogen

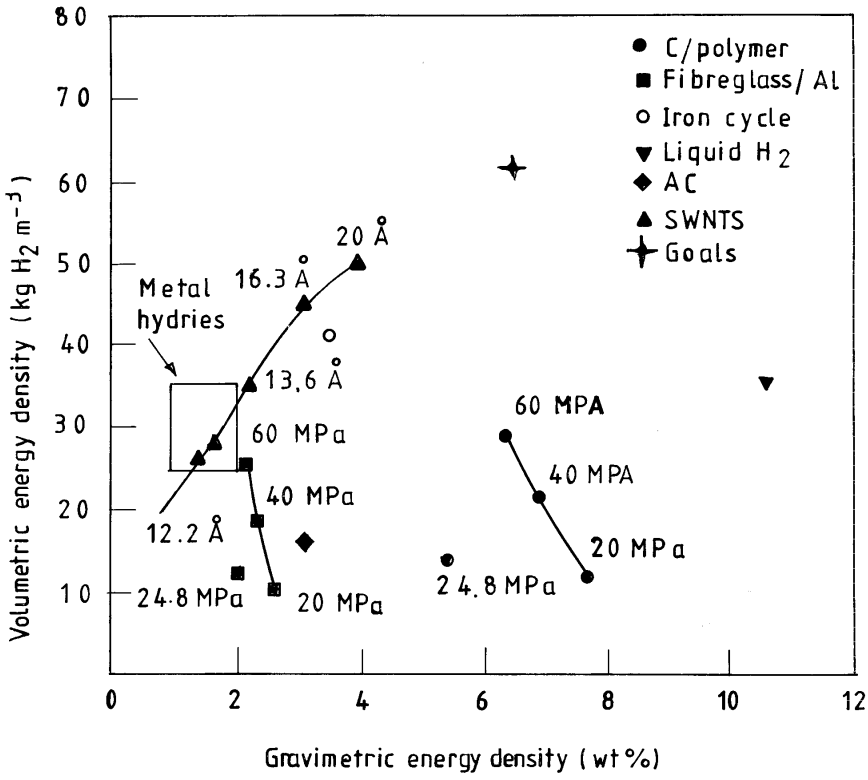

Figure 10.10 Installed energy densities for several vehicular hydrogen storage technologies[27]

storage. Liquid, compressed gas and reformer-derived hydrogen, all have well-known disadvantages. Extensive efforts have been made to develop methods for hydrogen storage, including metal hydrides and more recently, nano-structured carbons. Until recently, the development of a high capacity, lightweight material that could be used to reversibly store hydrogen under ambient conditions, seemed all but attainable.

10.4.5 Hydrogen in metals

In its molecular form, H_2 is too large to diffuse interstitially in most metals, neither can it readily cross the gas/metal interface in the molecular form. If the metal is molten, molecular hydrogen can dissolve readily, but it dissociates once in solution and can be retained as a mono-atomic solute on solidification.

If the material is solid, some mechanism to generate mono-atomic hydrogen at the gas/metal interface is necessary. Known mechanisms will be discussed here.

Whilst an interstitial solute, hydrogen remains in the mono-atomic form and is relatively mobile, even at ambient temperatures. However, to maintain such a mobile atom as an interstitial solute

presents problems in metals. Although crystalline, they are far from perfect, and lattice defects present areas where the lattice strain induced by the solute hydrogen atom is reduced, and thus tend to act as hydrogen traps.

When it is so trapped, the hydrogen atom becomes relatively immobile, but it is thought to remain as a single atom. If the trap site is a vacancy, the presence of a single hydrogen atom will lower the lattice strain due to the vacancy, and the hydrogen atom becomes a substitutional, rather than an interstitial, solute.

If the trap is a line defect, which is more likely due to their larger size and thus better accommodation, there may well accumulate a string of hydrogen atoms along the defect. The presence of a string of individual hydrogen atoms would not immobilise a dislocation, although it would increase the applied stress needed for movement. However, if two adjacent atoms on a line defect recombine to form molecular hydrogen, the applied stress required to cause movement becomes greater, effectively pinning the dislocation at that point. Since dislocation movement is the underlying process to plastic flow, the ductility of the material is reduced and the probability of brittle failure increased by the presence of hydrogen. In this context, interfaces such as grain boundaries or second phases should be considered as dislocation arrays, and thus are likely to accumulate solute hydrogen, quite possibly in molecular form, embrittling the interface. In addition to reducing the mobility of dislocations, solute hydrogen can also react, either with the solvent metal to form a hydride, or with some other solute element to form a new phase.

Molecular hydrogen gas can readily enter a molten metal surface, often added accidentally, as water contained in fluxes, mould dressings and alloying additions, dissociating into the mono-atomic form on dissolution, and remaining as a mono-atomic solute on solidification.

The diatomic hydrogen molecule is too large to enter the surface of a solid metal, and must be dissociated into single atoms. Two mechanisms for this are known—electrochemical and chemisorption.

The electrochemical evolution of atomic hydrogen is part of the cathode reaction in either a corrosion cell or an electroplating process. In addition, these can include such processes as acid cleaning and cathodic protection systems. As corrosion is essentially an electrochemical mechanism, both are sufficiently similar to be considered identical for the purpose of hydrogen evolution, and take the form:

$$M + H_2O \rightarrow MO + 2H \tag{10.4}$$

Most of the hydrogen atoms thus formed quickly combine to form diatomic gaseous hydrogen, but a portion of it enters the metal surface and remains as individual atoms in solution.

Dissociation of hydrogen by chemisorption is a rather different mechanism, and is well described by Christmann.[28] As a hydrogen molecule approaches a metal surface, weak van Der Waal's forces begin to act upon it, drawing it closer.

10.4.6 Metal hydrides

Hydrogen reacts at elevated temperatures with many transition metals and their alloys to form hydrides. The electropositive elements are the most reactive, that is, Sc, Yt, lanthanides and

actinides members of the Ti and V groups. The binary hydrides of the transition metals are predominantly metallic in character and are usually referred to as metallic hydrides. They are good conductors, have a metallic or graphite-like appearance, and can often be wetted by Hg.

Many of these compounds, (MH_n), show large deviations from ideal stoichiometry ($n = 1, 2, 3$) and can exist as multi-phase systems. The lattice structure is that of a typical metal with hydrogen atoms on the interstitial sites; and for this reason they are also called interstitial hydrides. This type of structure is limited to the compositions MH, MH_2, and MH_3, with the hydrogen atoms fitting into octahedral or tetrahedral holes in the metal lattice, or a combination of the two. The hydrogen carries a partial negative charge, depending on the metal, but an exception[29] is $PdH_{0.7}$. Pt and Ru are able to adsorb considerable quantities of hydrogen, which becomes activated. These two elements, together with Pd and Ni, are extremely good hydrogenation catalysts, although they do not form hydrides.[30]

Especially interesting are the metallic hydrides of intermetallic compounds, in the simplest case, the ternary system AB_xH_n, because the variation of the elements allows the properties of these hydrides to be tailored. Element A is usually a rare earth or an alkaline earth metal and tends to form a stable hydride. Element B is often a transition metal and forms only unstable hydrides. Some well-defined ratios of B/A, where $x = 0.5, 1, 2, 5$, have been found to form hydrides with a hydrogen to metal ratio of upto two.

The reaction of hydrogen gas with a metal is called the absorption process and can be described in terms of a simplified one-dimensional potential energy curve[31] (Fig. 10.11). The hydrogen atoms contribute their electron to the band structure of the metal. At a small hydrogen to metal ratio (H/M < 0.1), the hydrogen is exothermically dissolved in the metal (solid-solution, α-phase). The metal lattice volume expands proportional to the hydrogen concentration by approximately 2–3 $Å^3$ per hydrogen atom.[32]

At greater hydrogen concentrations in the host metal (H/M > 0.1), a strong hydrogen–hydrogen interaction becomes important because of the lattice expansion, and the hydride phase (β -phase) nucleates and grows. The hydrogen concentration in the hydride phase is often found to be H/M = 1. The volume expansion between the coexisting α- and β-phases corresponds, in many cases, to 10%–20% of the metal lattice. At the phase boundary, therefore, a large stress builds up and often leads to a decrepitation of brittle host metals such as intermetallic compounds. The final hydride is a powder with a typical particle size of 10–100 μm.

The thermodynamic aspects of hydride formation from gaseous hydrogen are described by pressure–composition isotherms (Fig. 10.12). When solid solution and hydride phases coexist, there is a plateau in the isotherms, the length of which determines the amount of hydrogen stored. In the pure β-phase, the hydrogen pressure rises steeply with the concentration. The two-phase region ends in a critical point, T_c, above which the transition from the α- to β-phase is continuous. The equilibrium pressure, p_{eq}, is related to the changes ΔH and ΔS in enthalpy and entropy, respectively, as a function of temperature by the Van't Hoff equation:

$$\ln (P_{eq}/P^{\circ}_{eq}) = (\Delta H/R \times 1/T) - \Delta S/R \tag{10.5}$$

As the entropy change corresponds mostly to the change from molecular hydrogen gas to dissolved solid hydrogen, it is approximately the standard entropy of hydrogen ($S_0 = 130\,\mathrm{J\,K^{-1}mol^{-1}}$) and is, therefore, $\Delta S_f \acute{\alpha} \approx -130\,\mathrm{J\,K^{-1}mol^{-1}H_2}$ for all metal-hydrogen systems. The enthalpy

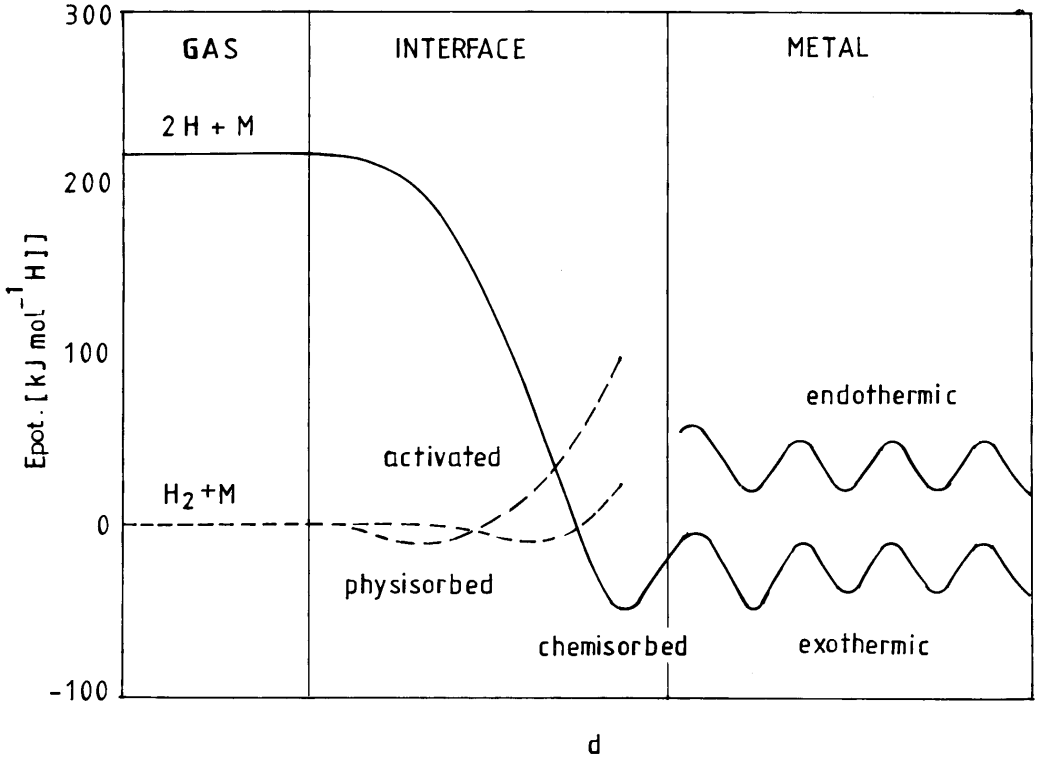

Figure 10.11 Far from the metal surface, the potential of a hydrogen molecule and of two hydrogen atoms are separated by the dissociation energy ($H_2 \rightarrow 2H$, $E_D = 435.99\,kJ\,mol^{-1}$). The first attractive interaction of the hydrogen molecule approaching the metal surface is the Van der Waals force leading to the physisorbed state ($E_{Phys} \approx 10\,kJ^{-1}$) approximately one hydrogen molecule radius ($\approx 0.2\,nm$) from the metal surface. Closer to the surface, the hydrogen has to overcome an activation barrier for dissociation and formation of the hydrogen metal bond. The height of the activation barrier depends on the surface elements involved. Hydrogen atoms sharing their electron with the metal atoms at the surface are then in the chemisorbed state ($E_{Chem} \approx 50\,kJ^{-1}\ H_2$). The chemisorbed hydrogen atoms may have a high surface mobility, interact with each other, and form surface phases at sufficiently high coverage. In the next step, the chemisorbed hydrogen atom can jump in the subsurface layer and finally diffuse on the interstitial sites through the host metal lattice

term characterizes the stability of the metal hydrogen bond. To reach an equilibrium pressure of 1 bar at 300 K, ΔH should amount to $39.2\,kJ\,mol^{-1}H_2$. The entropy of formation term for metal hydrides leads to a significant heat evolution $\Delta Q = T\Delta S$ (exothermal reaction) during hydrogen absorption. The same heat has to be provided to the metal hydride to desorb the hydrogen (endothermal reaction). If the hydrogen desorbs below RT, this heat can be delivered by the environment. However, if the desorption is carried out above RT, the necessary heat has to be

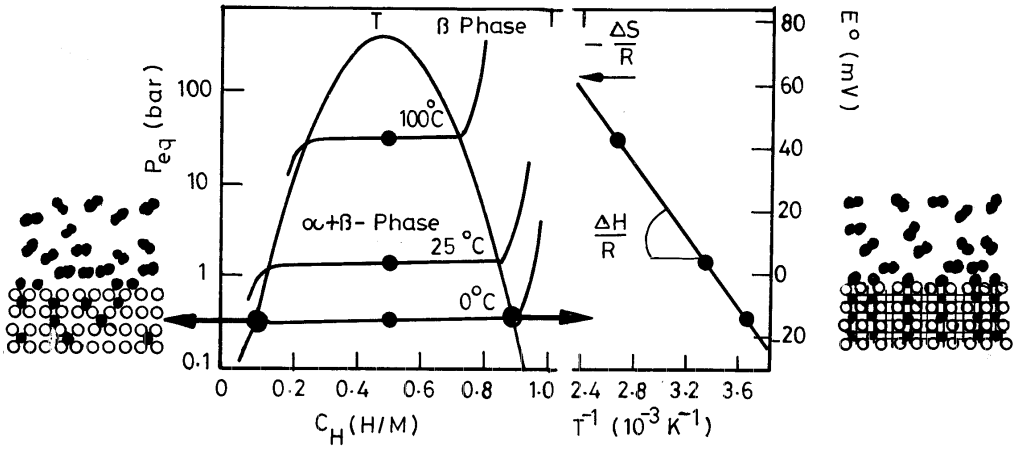

Figure 10.12 Pressure composition isotherms for hydrogen absorption in a typical intermetallic compound on the left hand side. The solid solution (α-phase), the hydride phase (β-phase) and the region of the co-existence of the two phases are shown. The co-existence region is characterized by the flat plateau and ends at the critical temperature T_c. The construction of the van't Hoff plot is shown on the right hand side. The slope of the line is equal to the enthalpy of formation divided by the gas constant and the intercept is equal to the entropy of formation divided by the gas constant

delivered from an external source, such as the combustion of hydrogen. For a stable hydride like MgH_2, the heat necessary for the desorption of hydrogen at 300 °C and 1 bar is $\approx$ 25% of the higher heating value of hydrogen.

Several empirical models allow the estimation of the stability and concentration of hydrogen in an intermetallic hydride. The maximum amount of hydrogen in the hydride phase is given by the number of interstitial sites in the intermetallic compound.[33,34] As a general rule, it can be stated that all elements with an electronegativity in the range of 1.35–1.82 do not form stable hydrides (hydride gap).[35] Here, the stability of a hydrogen atom on an interstitial site is the weighted average of the stability of the corresponding binary hydrides of the neighbouring metallic atoms.[36] More general is the Miedema model: the more stable an intermetallic compound, the less stable the corresponding hydride and vice versa.[37]

These semiempirical models allow estimation of the stability of binary hydrides as long as the rigid band theory can be applied. However, the interaction of hydrogen with the electronic structure of the host metal is often more complicated. In many cases, the crystal structure of the host metal and, therefore, the electronic structure, changes upon the phase transition and the theoretical calculation of the stability of the hydride becomes very complex, if not impossible. The stability of metal hydrides is usually presented in the form of Van't Hoff plots according to (10.6) (Fig. 10.13). The most stable binary hydrides have enthalpies of formation of $\Delta H_f = -226\,\text{kJ mol}^{-1}\text{H}_2$, example, HoH_2. The least stable hydrides are $FeH_{0.5}$, $NiH_{0.5}$ and $MoH_{0.5}$ with enthalpies of formation of $\Delta H_f = +20\,\text{kJ mol}^{-1}\text{H}_2$, $\Delta H_f = +20\,\text{kJ mol}^{-1}\text{H}_2$, and $\Delta H_f = +92\,\text{kJ mol}^{-1}\text{H}_2$, respectively.[38]

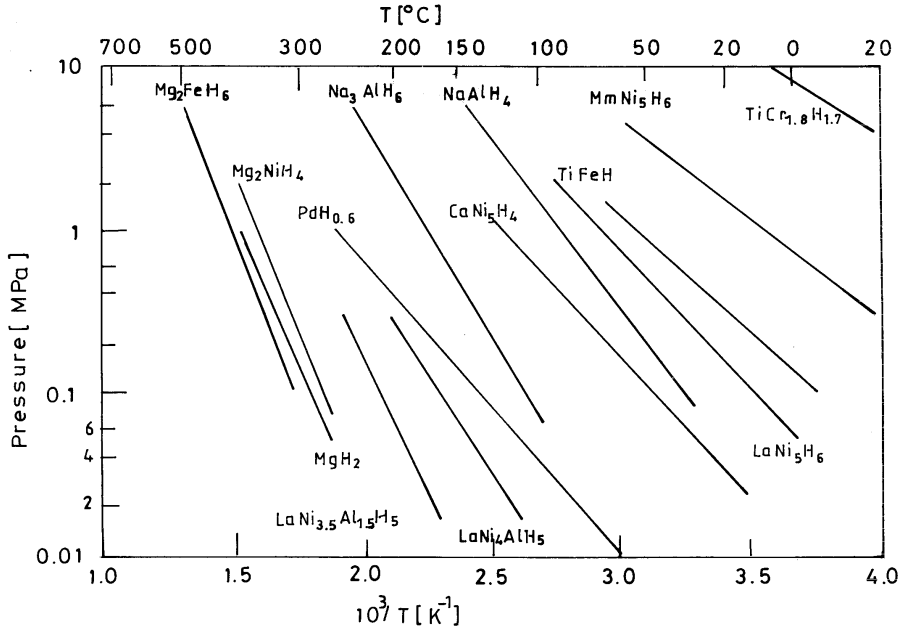

Figure 10.13 van't Hoff plots of some selected hydrides. The stabilization of the hydride of $LaNi_5$ by the partial substitution of Ni with Al in $LaNi_5$ is shown, as well as the substitution of La with mischmetal (example, 51% La, 33% Ce, 12% Nd, 4% Pr)

Because of this phase transition, metal hydrides, can absorb large amounts of hydrogen at a constant pressure, that is, the pressure does not increase with the amount of hydrogen absorbed. The characteristics of hydrogen absorption and desorption can be tailored by partial substitution of the constituent elements in the host lattice. Some metal hydrides absorb and desorb hydrogen at ambient temperatures close to atmospheric pressure. Several families of intermetallic compounds listed in Table 10.4 are interesting for hydrogen storage. They all consist of an element with a

Table 10.4 The most important families of hydride-forming intermetallic compounds, including the prototype and the structure. Element *A* has a high affinity to hydrogen and element *B* has a low affinity to hydrogen

Intermetallic compound	Protoype	Structure
AB_5	$LaNi_5$	Haucke phases, hexagonal
AB_2	ZrV_2, $ZrMn_2$, $TiMn_2$	Laves phase, hexagonal or cubic
AB_3	$CeNi_3$, YFe_3	Hexagonal, $PuNi_3$-typ
A_2B_7	Y_2Ni_7, Th_2Fe_7	Hexagonal, Ce_2Ni_7-typ
A_6B_{23}	Y_6Fe_{23}	Cubic, Th_6Mn_23-typ
AB	TiFe, ZrNi	Cubic, CsCl- or CrB-typ
A_2B	Mg_2Ni, Ti_2Ni	Cubic, $MoSi_2$– or Ti_2Ni-typ

high affinity to hydrogen, element *A*, and a low affinity one, element *B*. The latter is often at least partially Ni, since it is an excellent catalyst for hydrogen dissociation.

One of the most interesting features of metallic hydrides is the extremely high volumetric density of hydrogen atoms present in the host lattice. The highest volumetric hydrogen density reported to date is 150 kg m^{-3} in Mg_2FeH_6 and $Al(BH_4)_3$. Both hydrides belong to the complex hydrides family. Metallic hydrides can reach a volumetric hydrogen density of 115 kg m^{-3}, example, $LaNi_5$. Most metallic hydrides absorb hydrogen upto a hydrogen-to-metal ratio of H/M = 2. Greater ratios up to H/M = 4.5, example, for $BaReH_9$, have been found.[39] However, all hydrides with a hydrogen-to-metal ratio of more than two are ionic or covalent compounds and belong to the complex hydrides group.

Metal hydrides are very effective at storing large amounts of hydrogen in a safe and compact way. All the reversible hydrides working around ambient temperature and atmospheric pressure consist of transition metals; therefore, the gravimetric hydrogen density is limited to less than 3 mass%. It remains a challenge to explore the properties of the lightweight metal hydrides.

10.4.7 Complex hydrides

Light metals of group 1, 2 and 3, example, Li, Mg, B and Al, give rise to a large variety of metal-hydrogen complexes. They are especially interesting because of their light weight and the number of hydrogen atoms per metal atom, which is two in many cases. The main difference between the complex and metallic hydrides is the transition to an ionic or covalent compound upon hydrogen absorption. The hydrogen in the complex hydrides is often located in the corners of a tetrahedron with B or Al in the centre. The negative charge of the anion, $[BH_4]^-$ and $[AlH_4]^-$, is compensated by a cation, like, Li or Na. The hydride complexes of borane, the tetrahydroborates $M(BH_4)$ and the tetrahydroaluminates $M(AlH_4)$ are interesting storage materials. They are known to be stable and decompose only at elevated temperatures, often above the melting point of the complex.

Chemical or complex hydrides, such as $NaAlH_4$ and $NaBH_4$, are relatively new to the transportation market as they were thought to release hydrogen irreversibly at conditions outside the desirable temperature and pressure ranges. This 'misconception' changed abruptly with two technological breakthroughs. One was a US patent[40] in which Millennium Cell Inc. claimed that $NaBH_4$, when combined with a catalyst in an aqueous solution above pH 7, releases hydrogen at conditions suitable for use in passenger vehicles. As a result, one major automaker is pursuing limited commercialization of this technology. However, as exciting as this new hydrogen storage technology may appear, one major drawback is the prohibitively high cost of off-board reprocessing of the resulting borax solution back to $NaBH_4$. It is also not clear whether the gravimetric density of the Millennium Cell system meets any of the FreedomCar goals, especially those for 2015.

The second breakthrough with complex hydrides does not require off-board processing and allows hydrogen to be stored reversibly in a manner akin to metal hydrides. In 1996, the pioneering work of Bogdanovic and Schwickardi[41] showed, for the first time, adsorption and desorption pressure-concentration isotherms for catalyzed $NaAlH_4$ at temperatures of 180 °C and 210 °C. The isotherms, which have a nearly horizontal pressure plateau, do not show hysteresis. Furthermore, the catalyzed system reversibly absorbs and desorbs hydrogen of upto 4.2 mass%. The mechanism of the two-step reaction was also described. A more detailed study of $NaAlH_4$ with an improved

catalyst has been conducted more recently.[42] A desorption hydrogen pressure of 2 bar at 60 °C was found and the enthalpy for the dissociation reaction was determined to be 37 kJ mol^{-1} and 47 kJ mol^{-1} for the first and second dissociation steps of Ti-doped $NaAlH_4$, respectively, according to the reactions:

$$NaAlH_4 \leftrightarrow 1/3Na_3AlH_6 + 2/3Al + H_2 \qquad (3.7\,wt\%) \qquad (10.6)$$

$$Na_3AlH_6 \leftrightarrow 3NaH + Al + 3/2H_2 \qquad (3.0\,wt\%) \qquad (10.7)$$

The equilibrium hydrogen pressure at RT, therefore, is approximately 1 bar. Furthermore, the reaction is reversible–a complete conversion to product was achieved at 270 °C under 175 bar hydrogen pressure in 2–3 hours.[43]

The compound with the highest gravimetric hydrogen density at RT known today is $LiBH_4$ (18 mass%). This complex hydride could, therefore, be the ideal hydrogen storage material for mobile applications. $LiBH_4$ desorbs three of the four hydrogens in the compound upon melting at 280 °C and decomposes into LiH and B. The desorption process can be catalyzed by adding SiO_2, and significant thermal desorption has been observed,[44] starting at 100 °C. The stability of metal tetrahydroborides has been discussed in relation to their percentage ionic character, and those compounds with less ionic character than diborane are expected to be highly unstable.[45] Steric effects have also been suggested to be important in some compounds.[46,47] The special feature exhibited by covalent metal hydroborides is that the hydroboride group is bonded to the metal atom by bridging hydrogen atoms, similar to the bonding in diborane, which may be regarded as the simplest of the so-called 'electron-deficient' molecules. Such molecules possess fewer electrons than apparently required to fill all the bonding orbitals, based on the criterion that a normal bonding orbital involving two atoms contains two electrons. The molecular orbital bonding scheme for diborane has been discussed.[48]

Some of the common complex hydrides are listed in Table 10.5.[48] Clearly, only a paucity of the complex hydrides listed in Table 10.5 are currently being studied, essentially those that are

Table 10.5 Common complex hydrides for hydrogen storage applications[47]

Hydride	Mass% hydrogen	Availability
$KAlH_4$	5.8	*J.Alloys compd.*(2003) **353**,310
$LiAlH_4$	10.6	Commercially available
$LiBH_4$	18.5	Commercially available
$Al(BH_4)_3$	16.9	*J. Am. Chem. Soc.*(1953) **75**,209
$LiAlH_2(BH_4)_2$	15.3	British patents 840 572, 863 491
$Mg(AlH_4)_2$	9.3	*Inorg. Chem.*(1970) **9**,325
$Mg(BH_4)_2$	14.9	*Inorg. Chem.*(1972) **11**,929
$Ca(AlH_4)_2$	7.9	*J. Inorg. Nucl. Chem.*(1922) **1**,317
$NaAlH_4$	7.5	Commercially available
$NaBH_4$	10.6	Commercially available
$Ti(BH_4)_3$	13.1	*J.Am. Chem. Soc.*(1949) **71**,2488
$Zr(BH_4)_3$	8.9	*J.Am. Chem. Soc.*(1949) **71**,2488

[a] *Mass% of hydrogen in each molecule is based on theoretical maximum*

commercially available.[49,50] Much work has been carried out based on Bogdanovic's work on metal doped $NaAlH_4$, which showed that Ti-doped $NaAlH_4$ can decompose at 80–85 °C lower than the pure material. Although the first reaction generates only 3.7 mass% hydrogen at most and the second is limited to 1.9 mass% (a total of 5.6 mass% compared with 7.5 mass% in Table 10.5), this generated a great deal of excitement in the hydrogen storage community. For the first time, a complex hydride exhibited reversible hydrogen storage properties and reasonable capacities (similar to those of metal hydrides) at conditions commensurate with on-board storage and regeneration. Most researchers thought this was impossible.

The next breakthrough with complex hydrides was made by Jensen, Zidan and coworkers.[51,52] They showed that the decomposition temperature of Ti-doped $NaAlH_4$ can be further lowered using a high energy ball milling process to prepare the doped sample. Not only did this bring the conditions closer to those desired for on-board hydrogen storage, it also ignited the metal hydride research community to look at this novel, reversible complex hydride.

Another important discovery was the effect of doping $NaAlH_4$ with Ti-Fe[42,53] or Ti-Zr,[52,53] which lowers decomposition temperatures compared to using Ti, Zr, or Fe alone, as shown in Fig. 10.14.[53] Bogdanovic et al[41] and, recently, Wang et al, have shown that capacity losses from recycling can be alleviated by the addition of Al powder to the Ti-doped sample.[53] Also, an

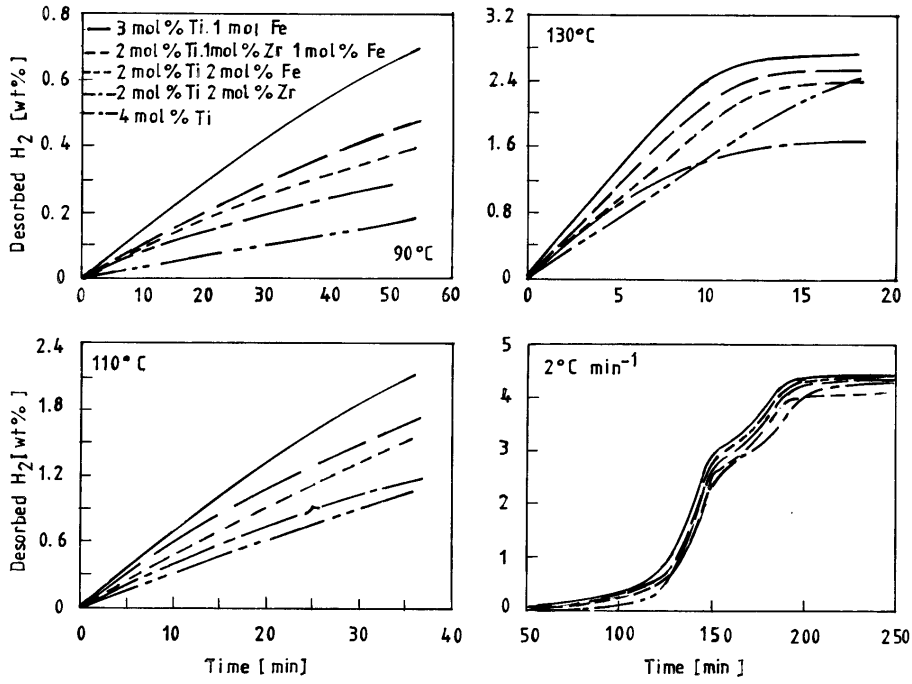

Figure 10.14 Constant temperature (90, 110, and 130 °C) and varying temperature 0th cycle thermogravimetric (2 °C/min) dehydrogenations of $NaAlH_4$ doped with 4 mol% Ti, Ti-Zr, Ti-Fe, Ti-Zr-Fe, and Ti-Fe, showing the synergistic behaviour of Ti-Fe and Ti-Zr over Ti alone[53–55]

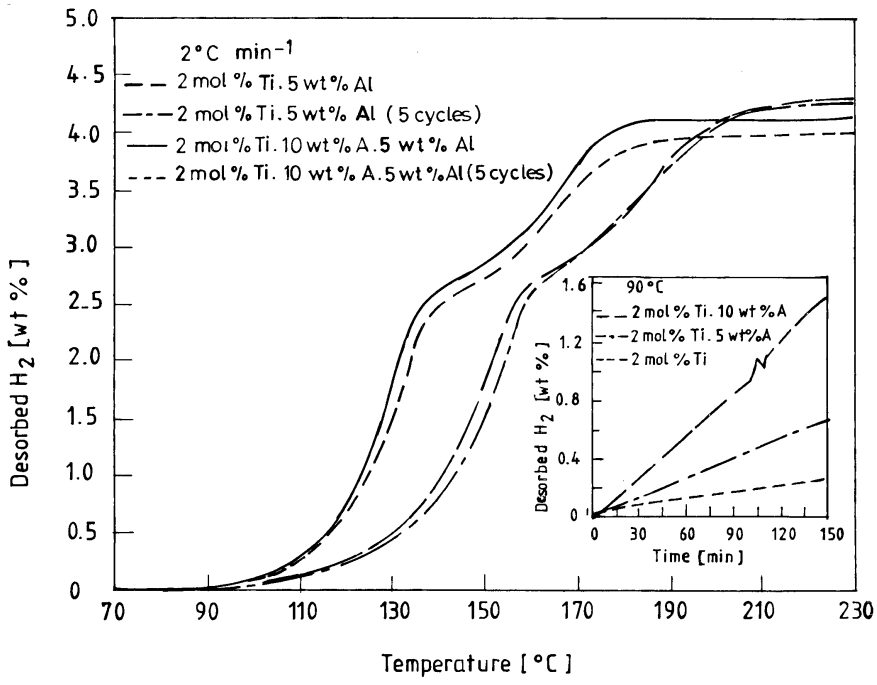

Figure 10.15 Varying temperature thermogravimetric (2 °C/min) dehydrogenations of $NaAlH_4$ doped with 2 mol% Ti and 5 wt% Al powder with and without 10 wt% proprietary additive. Initially (0th cycle) and after five rehydrogenation cycles (at 150 °C and 100 atm for 2 hrs), the Al powder eliminates cycle losses, while the proprietary additive improves the dehydrogenation conditions.[55] The insert reveals the effect of the proprietary additive when added to $NaAlH_4$ doped with 2 mol% Ti in 5 wt% and 10 wt% amounts during 0th cycle constant temperature (90 °C) thermogravimetric dehydrogenations.[55]

improvement in the decomposition rate and temperature has been achieved using a proprietary additive with Ti-doped $NaAlH_4$; the additive works even when Al is added to minimize cycling losses, as shown in Fig. 10.15.[53]

Other results are piecing together the mechanistic role of the metal dopant in promoting the thermodynamic and kinetic uptake and release of hydrogen by $NaAlH_4$. For example, *X*-ray diffraction (XRD) and solid-state NMR studies show that the loss of hydrogen capacity upon recycling is the result of unreacted Al preventing reaction (10.7) to reverse completely.[41] In addition, studies using in situ XRD, scanning electron microscopy, energy dispersive spectroscopy, and Auger spectra analysis show that most of the metal dopant remains at the sample surface.[54–59] Long-range transport of the metal species during the dehydriding process has also been discovered, where Al is possibly being transported to and segregating at the surface during rehydrogenation, with speculation that the transported species may be a more mobile hydride, such as AlH_3.[55–57] In situ XRD studies reveal that the doping process alters certain lattice parameters, inducing distortion that reaches a maximum when $NaAlH_4$ is doped with 2 mol% Ti.[54] This not only provides crucial evidence on the

role of Ti in improving hydrogen transport via lattice distortion, but also indicates that 2 mol% Ti may be close to the optimum dopant level. X-ray photoelectron spectroscopy studies of Ti-doped Li_3AlH_6 reveal that the surface Ti contains $Ti^0/Ti^{2+}/Ti^{3+}$ species.[60] This indicates that $Ti^0 \leftrightarrow Ti^{3+}(Ti^0/Ti^{2+}/Ti^3)$ defect site chemistry may play a role in enhancing the system's reversibility. Whether this applies to $NaAlH_4$ is not known, however. To assist in the search for the elusive mechanistic role of the metal dopant, Ritter et al[61] are carrying out molecular orbital calculations for the $LiAlH_4$ and $NaAlH_4$ systems and have evolved a total electron density map of $LiAlH_4$.

Although exciting discoveries are being made with some complex hydrides, especially Ti-doped $NaAlH_4$, and light is being shed on the role of Ti, a detailed mechanism based on definitive experimental evidence, is still lacking. Even Ti-doped $NaAlH_4$ with Al and the proprietary additive only provides 3 mass% reversible hydrogen at reasonable rates when discharged at $> 100\,^{\circ}C$. Although the additive improves the kinetics, the capacity is still too low for on-board passenger vehicles. Moreover, pressures of 1,500 psig are required to achieve reasonable rates during rehydrogenation. Even so, this is still not fast enough for on-board refuelling, unless temperatures exceed $110\,^{\circ}C$. Despite these limitations, Ti-doped $NaAlH_4$ is one of the best hydrogen storage materials known, surpassing all metal hydrides in release capacity.

Complex hydrides open a new field of hydrogen storage materials. While the alanates have been investigated extensively during the last six years, there is a whole field of new compounds ready to be explored. The borides are especially interesting because of their very high gravimetric and volumetric hydrogen density. Metal hydrides have been investigated for hydrogen storage since the 1970s, but no remarkable success has been achieved because of the low gravimetric densities that could be obtained for hydrogen in these intermetalics. Thus, the storage of this gas on board automobiles is a problem not solved to date and is the aim of many applied but fundamental research efforts today.

Several authors[62,63] have identified some of the essential requirements that should be satisfied by metal hydrides proposed for hydrogen storage at a commercial level. These are summarized below.

1. High hydrogen content;
2. Facile reversibility of formation and decomposition reactions. The hydride should be decomposable at moderate temperatures that can be provided from locally available heat sources, like solar, automobile exhaust and waste heat sources;
3. Absorption-desorption kinetics should be compatible with the charge-discharge requirements of the system;
4. The equilibrium dissociation pressure of the hydride at peak desorption rate should be compatible with the safety requirements of the hydride containment system. The hydride itself should have a high safety factor;
5. The hydride should have a sufficient chemical and dimensional stability to permit its being unchanged over a large number of charge–discharge cycles;
6. Minimal hysteresis in adsorption–desorption isotherms;
7. The hydride should be reasonably resistant to deactivation by low concentrations of common (sometimes unavoidable) contaminants such as O_2, H_2O, CO_2, CO, and others;
8. The total cost of hydride (raw materials, processing and production) should be affordable for the intended application. The long term availability of raw materials (that is, the

metal resources), must be ensured. The cost of the hydride system (which includes its containment) per unit of reversibly stored hydrogen should be as low as possible;

9. The storage vessel and ancillary equipment cost and the fabrication and installation costs should be moderate;
10. Operating and maintenance costs and purchased energy requirements (that is, energy other than waste energy and energy extracted from the ambient air) per storage cycle should be low.

A judicious combination of technical and economic considerations will determine the suitability of a hydride product for a given hydrogen storage or hydrogen containment application.

10.5 Prediction of Hydrogen Uptake in Carbon Materials

Carbon materials can be considered as one of the candidates for energy storage, because of a combination of adsorption ability, high specific surface, pore microstructure and low mass density. The three well-known forms of carbon are diamond, graphite and fullerenes. In diamond each carbon has four bonds to its neighbours and forms a three-dimensional lattice. Graphite is built up of two-dimensional hexagonal sheets of carbon atoms where the carbon–carbon distance in the plane is 1.42 Å and the distance between the sheets is 3.35 Å. The classic example of the difference between sp^3 and sp^2 bonding properties is how carbon forms diamond and graphite. For diamond, the three-dimensional, four-fold coordinated sp^3 structure is rigid and almost isotropic in its properties. In contrast, the graphite sp^2 bonding is planar and three-fold coordinated in the planes with weak bonding between the planes. The strong covalent in-plane bonding and weak van der Waals interplane bonding result in anisotropic physical properties which are useful for applications in lubrication and other processes requiring 'slippage' between layers. The in-plane carbon–carbon bonds are shorter than those of diamond, but the interlayer distance is large.

In the 1970s graphite nanofibers (GNFs) were discovered, which consist of graphite platelets stacked together in various orientations to the fiber axis with an interlayer spacing similar to bulk graphite. The length of these GNFs can vary between 5 and 100 μm and their diameter between 5 and 200 nm. In the configuration of GNFs with so-called herringbone type structure, the graphite sheets are stacked with a certain angle to the fiber axis, or conically shaped graphite sheets are stacked. In transmission electron microscopy investigations both structures yield in projection of a fish-bone like image.

In 1991, Iijima[64] described for the first time the new form of carbon called carbon nanotubes (CNT). CNTs are formed by rolled graphite sheets, with an inner diameter starting from 0.7 nm upto several nm and a length of 10–100 μm. The CNTs are described as usually closed on both sides by a hemisphere, that is, half of a fullerene. Tubes formed by only one single graphite layer are called single wall nanotubes (SWNT); tubes consisting of multiple concentric graphite layers are called multi-wall nanotubes (MWNT). The interlayer distance in MWNTs is closer to the interlayer distance in graphite, which is equal to half of the unit cell parameter c ($0.5c = 0.3355$ nm). The diameter of SWNTs varies from 0.671 to 3 nm, whereas MWNTs show typical diameters of 30–50 nm. The helicity of the nanotubes is usually described by the Hamada vector,[65] which indicates how the graphene sheet is rolled up along a lattice vector with components (n, m). The

values of the integers n and m identify the general geometry of SWNT. The tubes with $n = m$ are named 'armchair'; tubes with either $n = 0$ or $m = 0$ are named 'zigzag'; all others have chiral symmetry.[66,67] The schematic representation is given in Fig. 10.16. One can view a single-walled carbon tube as a rolled up sheet or strip of sp^2-bonded graphene. The atoms are located using a pair of integers (n, m) and the lattice vector $C = na_1 + ma_2$ as shown in Fig. 10.16. A tube can be classified using the pair of integers by viewing the rolling up of the sheet as the 'placement' of the atom at (0,0) on the atom at (n, m). Hence, different diameter tubes and helical arrangements of hexagons can arise by changing (n, m) as shown in Fig. 10.17 and Fig. 10.18.

SWNTs tend to agglomerate and form bundles of several tens of nanotubes. The nanotubes in the bundles are in 2-dimensions closed-packed and the intertube distance is 0.334 nm.[68] Carbon fibers and carbon nanotubes are similar materials except for their inner structure. Carbon fibers consist of graphite platelets stacked together with an interlayer spacing of 0.3355 nm in various orientations with respect to the fiber axis, giving rise to assorted conformations. Three types of carbon fibers can be distinguished. In the platelet-like carbon fiber, the area vector of the graphene sheets is parallel to the axis of the fiber. This type of fiber can be easily distinguished from nanotubes since they do not exhibit a concentric hole, that is, they are not tube like and the shadow lines in the TEM images are perpendicular to the fiber axis. The ribbon-like fibers consist of continuous graphene layers along the axis of the fiber. This type of fiber exhibits a very similar pattern in the TEM image just like the bundles of SWNTs. The herringbone fibers finally are an intermediate type and consist of graphite platelets with an area vector oriented 45° to the axis of the fiber (Fig. 10.19).

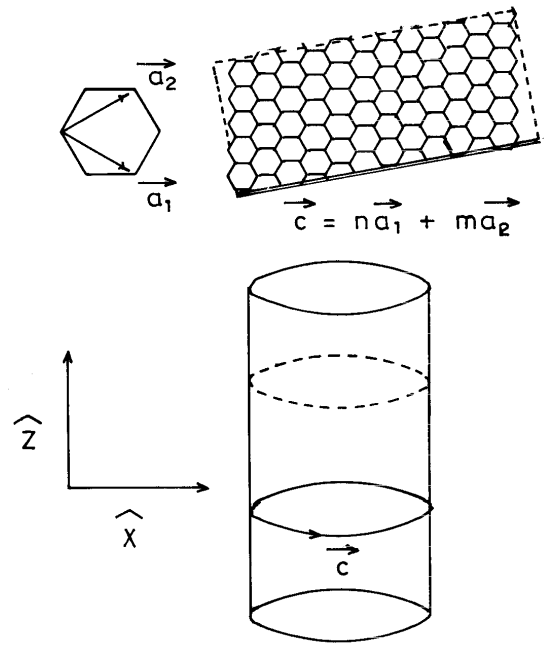

Figure 10.16 Structure of an (n, m) carbon nanotube: the carbon atoms are at the vertices of the hexagons [Reproduced from Ref. 67]

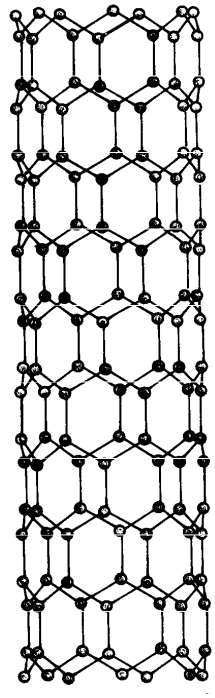

Figure 10.17 Ball and stick model for a nanotube: the balls represent carbon atoms [Reproduced from Ref. 67]

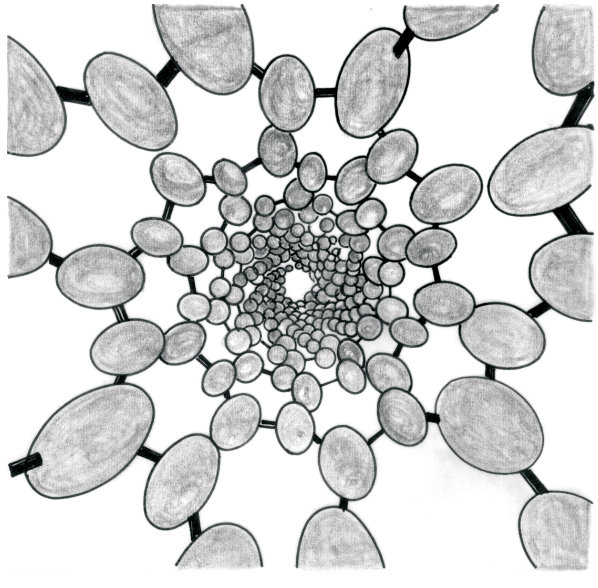

Figure 10.18 Schematic structural model of a helical nanotube [Reproduced from Ref. 67]

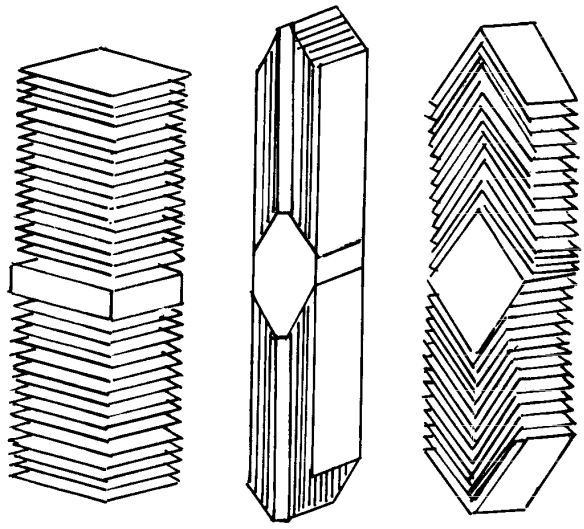

Figure 10.19 Schematic representation of the three forms of graphitic nanofibers: (a) platelet (b) ribbon (c) herringbone structures

Among nanostructures, tubular materials are especially interesting because their morphology is assisted with an intrinsic multifunctionality that arises from four different contact regions as tube opening, outer surface, inner surface and interestial region. These properties render nanotubes as promising candidates for the realization of highly functional, effective and resource saving nanodevices such as sensors, capacitors or storage and release systems.

However, there is still an important search for new or optimized carbons, especially with well-controlled nanostructure and surface functionality, in order to improve the storage capacity and the cycleability of the power supply. Carbon nanotubes have been carefully examined for all these applications, where their unique morphology (helical or fishbone arrangement of graphitic layers, presence of a central canal, entanglement, bundles formation) is expected to be profitable for improved performance. The mesoporous character of carbon nanotubes plays a dominant role in their electrochemical properties. Compared to conventional carbon materials, carbon nanotubes show higher rate of electron transfer. Their entangled network and central canal are at the origin of pseudocapacitive effects, allowing an easy access of the ions to the electrode/electrolyte interface. Multi-walled nanotubes or nanofilaments (MWNTs) and single-walled nanotubes (SWNTs) have been used for lithium storage,[69–74] electrochemical capacitors,[75–79] and electrochemical hydrogen storage[80,81] and for promoting some redox reactions[82,83] applicable for fuel cells.

Due to its high surface area and abundant pore volume, porous carbon is considered as a good adsorbent. For conventional porous carbon, the hydrogen uptake is proportional to its surface area and pore volume, while, regretfully, a high hydrogen adsorption capacity ($4 \sim 6$ wt%) can be obtained only at very low temperatures such as liquid nitrogen temperature,[84] consistent with theoretical calculations. In contrast, in spite of their relatively small surface area and pore

volume, carbon nanotubes and carbon nanofibers surprisingly show very high hydrogen storage capacity. Scientists employed different theoretical calculations and deductions in search of a reasonable interpretation. The intent of these theoretical studies is to find answers to the following questions:

1. How do structural characteristics influence the physical/chemical process?
2. Where does the adsorption occur? In inner hollow cavities and in other pore space (inter-tube space) or in only one of them?
3. In the adsorption of hydrogen onto carbon nanotubes, what interaction—chemical or physical—occurs between the hydrogen and the carbon?
4. What is the adsorption mechanism?
5. What is the maximum adsorption capacity?

10.5.1 Physisorption or chemisorption

Porous carbon is considered as a good adsorbent due to its high surface area and abundant pore volume. Specific pores can be anticipated in the bundles of single-walled carbon nanotubes. Hydrogen molecules can be located inside nanotubes or interstitially between them.

Resonant fluctuations in charge distributions, which are called dispersive or van der Waals interactions, are the origin of the physisorption of gas molecules onto the surface of a solid. In this process, a gas molecule interacts with several atoms at the surface of a solid. The interaction is composed of two terms: an attractive term, which diminishes with the distance between the molecule and the surface to the power of -6, and a repulsive term, which diminishes with distance to the power of -12. The potential energy of the molecule, therefore, shows a minimum at a distance of approximately one molecular radius of the adsorbate. The energy minimum is of the order of 0.01–0.1 eV (1–10 kJ mol^{-1}). Because of the weak interaction, significant physisorption is only observed at low temperatures (< 273 K).

Once a monolayer of adsorbate molecules is formed, gaseous molecules interact with the surface of the liquid or solid adsorbate. The binding energy of the second layer of adsorbate molecules is, therefore, similar to the latent heat of sublimation or vapourization of the adsorbate. Consequently, a single monolayer is adsorbed at a temperature equal to or greater than the boiling point of the adsorbate at a given pressure. To estimate the quantity of adsorbate in the monolayer, the density of the liquid adsorbate and the volume of the molecule is required. If the liquid is assumed to consist of a close-packed, face-centred cubic structure, the minimum surface area, S^{ml}, for one mole of adsorbate in a monolayer on a substrate can be calculated from the density of the liquid, ρ_{liq}, and the molecular mass of the adsorbate, M_{ads}:

$$S^{ml} = \sqrt{\frac{3}{2}}\left(\sqrt{\frac{2}{N_A}} \times \frac{M_{\text{ads}}}{\rho_{\text{liq}}}\right) \tag{10.8}$$

where N_A is the Avogadro constant. The monolayer surface area for hydrogen is $S^{ml}(\text{H}_2) = 85\,917\,\text{m}^2\text{mol}^{-1}$. The amount of adsorbate, m_{ads}, on a substrate material with specific surface

area, S_{spec}, is given by $m_{ads} = M_{ads} S_{spec}/S^{ml}$. In the case of carbon as the substrate and hydrogen as the adsorbate, the maximum specific surface area of carbon is $S_{spec} = 1315\,m^2g^{-1}$ (single-sided graphene sheet) and the maximum amount of adsorbed hydrogen is $m_{ads} = 3.0$ mass%. From this approximation, one can conclude that the amount of adsorbed hydrogen is proportional to the specific surface area of the adsorbent with $m_{ads}/S_{spec} = 2.27 \times 10^{-3}$ mass% $m^{-2}g$, and can only be observed at very low temperatures.

Materials with a large specific surface area like activated or nanostructured carbon and carbon nanotubes (CNTs) are possible substrates for physisorption. The main difference between CNTs and high surface area graphite is the curvature of the graphene sheets and the cavity inside the tube. In microporous solids with capillaries, which have a width of less than a few molecular diameters, the potential fields from opposite walls overlap so that the attractive force acting upon adsorbate molecules is increased compared with that on a flat carbon surface.[85] This phenomenon is the main motivation for the investigation of the hydrogen-CNT interaction.

The adsorption of hydrogen in carbonaceous materials corresponds to the amount of hydrogen adsorption which takes place near the carbon solid surface due to the physical forces—van der Waals interactions. In long SWNTs closed with fullerene-like caps at the end, the hydrogen can only get access to the interior of the tube via the six-membered ring of the graphite-like tube wall. An opened tube with removed caps may give an easier access for the hydrogen molecule into the tube. Typically, the tubes are very long and therefore a good diffusivity of the hydrogen inside the tube will be required in order to fill the whole tube volume. Furthermore, one can imagine that a structural defect in the tube or a sharp bend of the tube may block the hydrogen diffusion. Therefore, cutting the tubes in shorter pieces may help to overcome this problem. The access from the side requires diffusion between the closest tube–tube distance whereas the interstitial sites are directly accessible from the rope ends. To fill the whole volume of these interstitial sites or better cylinders, owing to its extension in one dimension along the whole rope, will require good hydrogen diffusivity inside these cylinders. Again cutting the rope in short pieces may help to improve hydrogen storage and its kinetics.

It is known that hydrogen adsorbs at solid surfaces depending on the applied pressure and temperatures. The variation of attractive surface forces as a function of distance from the surface decides whether van der Waals-type weak physisorption of molecular hydrogen occurs, or whether dissociation and chemisorption of atomic hydrogen takes place. Owing to the attractive forces, the most stable position for an adsorbed molecule is with its centre at about one molecular radius from the surface, and the attractive field rapidly diminishes at greater distances. Once a monolayer of adsorbate molecules or atoms has formed, the gaseous species interact with the liquid or solid adsorbate. Therefore, the binding energy of the second layer of adsorbates is similar to the latent heat of sublimation or vapourization of the adsorbate. Consequently, adsorption at a temperature at or above the boiling point of the adsorbate at a given pressure leads to the adsorption of a single monolayer.

Are curved structures more attractive? In microporous solids with capillaries which have a width not exceeding a few molecular diameters (the diameter of H_2 is 0.41 nm), the potential fields from opposite walls overlap so that the attractive force acting on hydrogen molecules is greater than that on an open flat surface. The effect of nanotube curvature on the adsorption energy for hydrogen has been investigated theoritically by Stan and Cole.[86] The adsorption potential was found to be

9 kJ mol^{-1} for hydrogen molecules inside the nanotubes at 50 K, at about 25% higher than on the flat surface of graphite. The increase arises from the curvature of the surface and the related higher number of carbon atoms interacting with the hydrogen molecule. At low temperatures, far more hydrogen can be adsorbed in the tube than on a flat surface; but the ratio decreases strongly with the increasing temperature, from 55 at 50 K to 11 at 77 K.

Later, Lee et al[87] have carried out density functional calculations for hydrogen storage behaviour in SWNTs and proposed that the adsorption of hydrogen in SWNTs is a chemisorption process. Their calculation predicted that the hydrogen storage capacity in (10,10) nanotubes can exceed 14 wt% (160 kg H_2/m^3), the value higher than most of the experimental values.

10.5.2 Simplistic geometric estimate and qualitative discussion

Since H_2 molecules at elevated pressures on a solid surface are expected to form a close-packed configuration, Dresselhaus et al[88] obtained a simple geometric estimate for the close-packing capacity of hydrogen molecules above a plane of graphite using purely geometric arguments, which, for hydrogen uptake for one layer of H_2 adsorbed on a single graphene layer, yields 2.8 wt% ($\sqrt{3} \times \sqrt{3}$ commensurate stacking, Fig. 10.20, top) or 4.1 wt% (dense triangular structure, incommensurate with the graphite, observed for higher hydrogen pressure, Fig. 10.20, bottom).[88,91]

As for nanotubes, one important issue currently being debated is whether hydrogen adsorption also occurs in the interstitial channels between adjacent nanotubes in a rope of SWNTs. Dresselhaus et al[88] presented two geometrical estimates for the filling of a rope (crystalline lattice) of SWNTs. One assumes that hydrogen is a completely deformable fluid that fills the space not occupied by the carbon nanotubes, and the other is the packing of hydrogen molecules of kinetic diameter 0.29 nm

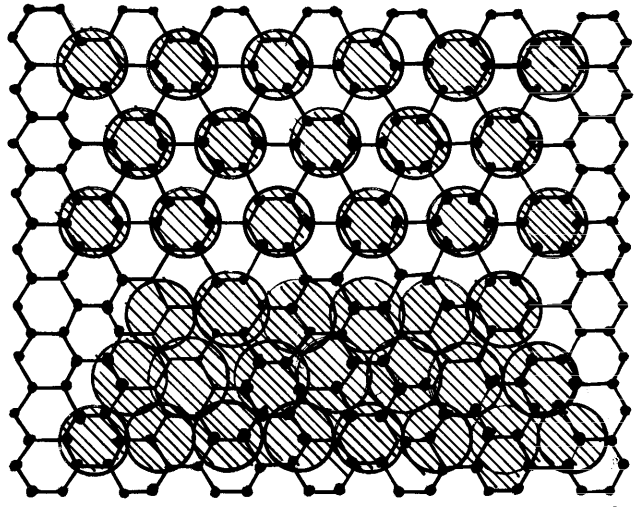

Figure 10.20 Relative density of $a \times$ commensurate (top) and an incommensurate (bottom) monolayer of H_2 on a graphite surface [Reproduced from Ref. 92]

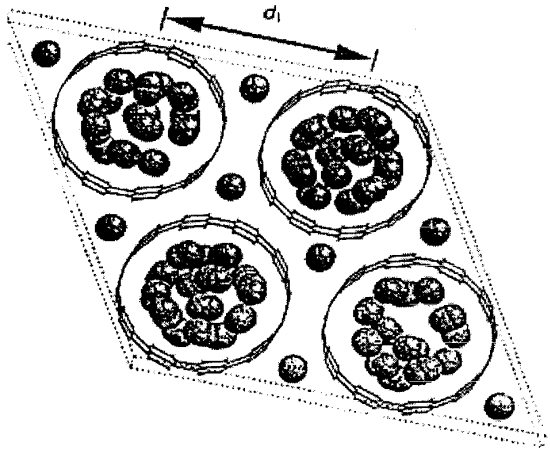

Figure 10.21 A typical configuration of H_2 molecules adsorbed on a triangular array of carbon nanotubes. This configuration resulted from a classical Monte Carlo calculation in which the simulated storage pressure was 10 MPa and the simulated temperature was 50 K. [Reproduced from Ref. 91]

on the inner walls and in the interstitial volume of the nanotubes, as shown in Fig. 10.21. Using the geometrical model with close-packing of hydrogen molecules within the core of a (10,10) tube leads to 3.3 wt% hydrogen adsorption within the tube and 0.7 wt% adsorption within the interstitial space, or a total of 4.0 wt% hydrogen adsorption.[88]

It is considered that under high-pressure conditions (example, 10 MPa), the high compressibility of hydrogen and the attractive intermolecular interactions should lead to closer packing of hydrogen molecules,[88] which is consistent with the calculations by Stan et al,[92] yielding a hydrogen density higher than the simple geometric picture. Based on this, the hydrogen adsorption amount under high pressures would be higher than the simplistic geometric estimate.

Moreover, Dresselhaus thought that a hydrogen molecule adsorbed in the interstitial space undergoes stronger surface attraction than on a single planar graphene surface, since it is in close proximity to three graphene surfaces.[88] Therefore, the hydrogen adsorbed in the space would be expected to be denser than on the single graphene surface.

In short, through a simple physical description, it is concluded that for SWNTs, hydrogen is stored in the pores formed by both, the inner tube cavities and the inter-tube space, and the storage density is possibly higher than that on a planar graphene surface. Accordingly, the hydrogen adsorption amount may be higher than 4 wt%, consistent with the experimental results.

10.5.3 Simulation for hydrogen adsorption onto carbon nanotubes

Carbon nanotubes have been known for more than a decade now. It is a challenge to fill the unique tubular structure of carbon nanotubes with metals and gases. Especially, the uptake of hydrogen in single wall nanotubes has attracted the attention of many research groups worldwide. The values

published for the quantity of hydrogen absorbed in nanostructured carbon materials vary between 0.4 and 67 mass%.

Many scientific publications are devoted to the theoretical study of physical adsorption of gases on different adsorbent structures. Among these, noble gases are widely studied due to the inertness of these gases near reactive surfaces such as graphite planes and the walls of carbon nanotubes. These studies concern both, theoretical and realistic models of molecular gases in pores described by hard walls or attractive interfaces. They established that the physical adsorption of gases on a solid adsorbent can be accurately computed by numerical simulation.[93–96] However, concerning carbon nanotubes, a few experimental studies have been devoted to measurements of gas adsorption on these adsorbents. The adsorption of diatomic gases such as hydrogen and nitrogen has been studied at different pressures and temperatures.[96–98]

Monte Carlo simulations[68,99–102] and other calculations[86,91,103,104,110] have been carried out to verify and predict the adsorption capacity of hydrogen in carbon nanotubes based on the assumption of physical adsorption (Monte Carlo numerical simulation is based on equilibrium statistical mechanics and corresponds to a thermodynamic evaluation of the amount of gas adsorbed near the adsorbent surface. For this calculation one needs the gas–adsorbent and gas–gas molecular interaction data). For all these approaches, the most important factor in the simulations is the choice of the intermolecular potential function describing the molecular interaction between hydrogen and carbon atoms. In spite of the use of different calculation methods, the following conclusions have been reached.

1. Williams and Eklund[99] performed Monte Carlo simulation of H_2 physisorption in finite-diameter carbon SWNT ropes and found an increasing amount of adsorbed hydrogen with decreasing temperature from 1.4 mass% ($p = 10$ MPa, $T = 300$ K) to 9.6 mass% ($p = 10$ MPa, $T = 77$ K). For lower hydrogen pressure this range is shifted to considerably lower amounts of adsorbed hydrogen, that is, 0.2 mass% ($p = 1$ MPa, $T = 300$ K) to 5.9 mass% ($p = 10$ MPa, $T = 77$ K).

   They have calculated the specific surface area (m^2 /g) accessible to a spherical 'probe' of diameter 2.8 Å (comparable to the kinetic diameter of H_2 under the conditions of interest) in ropes of different diameter. The van der Waals radius of carbon was taken to be 1.7 Å. In the simple method used for their study, the probe 'molecules' were rearranged about the surface of the host material (in this case, the SWNT rope) and the cell was loaded until a maximum number of probe molecules had been introduced into the simulation cell. The surface area was then deduced from the cross-sectional area of the probe molecule multiplied by the number of probe molecules which cover the host surface. The computation was done for the specific surface areas in the endohedral (denoted σ_{endo}), interstitial (σ_{inter}), and outer (σ_{outer}) adsorption sites in SWNT ropes composed of one to 37 nanotubes. A plot was made for σ_{TOT}, σ_{endo}, σ_{inter}, and σ_{outer} as a function of rope diameter. It was observed that by increasing the rope diameter, σ_{inter} slowly increases and approaches the value for an infinite lattice; of course, σ_{endo} is constant for all rope diameters. It was noted that σ_{outer} (and therefore σ_{TOT}) increases strongly with *decreasing* rope diameter. Thus, it was expected that the contribution of σ_{outer} to be important for small diameter ropes; in fact, the values for $\sigma_{outer} > \sigma_{endo}$ for rope diameters ≤ 5 nm,

which contain $\leq$ 7 SWNT. Therefore, it was proposed that for realistic calculations one must consider the gravimetric capacity of the 'outer' surface.

Quantitative examination of the maximum potential energies in a 7-SWNT rope at 10 MPa and 77 K showed that the strongest average attractive potential energy is in the interstices (−1,443 K), followed by the endohedral sites along the inner (−758 K) and outer (−603 K) cylindrical surface of the nanotubes. Further, the attractive potential energies along the 'grooves' (the wedge-shaped channel running along the outer surface of the rope where two nanotubes meet) is −1,088 K, comparable to the energy in the interstitial sites. These estimates suggest that treatment of the outer surface of SWNT ropes in the simulation of physisorption is important not only for the obvious geometrical reasons (high surface area), but for energetic reasons as well, since typical ropes possess many 'wedge' channels on their exterior surface.

2. Rzepka et al[100] used a grand canonical ensemble Monte Carlo programme to calculate the amount of absorbed hydrogen for a slit pore and a tubular geometry. The amount of absorbed hydrogen depends on the surface area of the sample and the maximum is at 0.6 mass% ($T = 300$ K, $p = 6$ MPa). The calculation was verified experimentally with an excellent agreement. At a temperature of 77 K the amount of absorbed hydrogen is about one order of magnitude higher when compared to 300 K.
3. Wang et al[101,102] have calculated the adsorption isotherms of hydrogen in arrays of SWNTs, isolated SWNTs, and idealized carbon slit pores. The inner-tube cavity has high adsorption potential for hydrogen, compared to the planar surface and slit-pores of similar size (Fig. 10.22). Figure 10.22 shows that the depth of the potential well for the (9, 9) tube (1.22 nm in diameter) array is larger than that for a slit pore 0.9 nm in diameter because the curvature of the tube increases the number of nearest neighbour carbon atoms.[102]

   Interstitial adsorption constitutes a significant fraction of the total amount adsorbed for a tube of larger diameter such as the (18, 18) (2.44 nm) tube array. By comparison, in the smaller interstices of the (9, 9) tube array, adsorption is negligible due to the quantum effect. The (18, 18) interstices show a local enhancement of potential energy. The minimum energy in the interstice is greater than that inside the (18, 18) tube by a factor of nearly 2. Interstitial adsorption accounts for, at most, 14% of the total adsorption for the (18, 18) tube array at 77 K.[102]
4. The packing geometry of the SWNTs plays an important role in hydrogen adsorption. The simulation of Williams et al[99] suggests strong dependence of the gravimetric adsorption on the packing geometry. The diameter of a SWNT rope correlates with computed values of the specific surface area, and delaminating of nanotube ropes should increase the gravimetric storage capacity.
5. Stan and Cole[86] used the Feynman (semiclassical) effective potential approximation to calculate the adsorption potential and the amount of hydrogen adsorbed on a zigzag nanotube (13, 0) with a diameter of 1.018 nm. The adsorption potential was found to be 9 kJ mol^{-1} for hydrogen molecules inside the nanotubes at 50 K. The potential is about 25% higher as compared to the flat surface of graphite due to the curvature of the surface and therefore, there is an increased number of carbon atoms interacting with the hydrogen

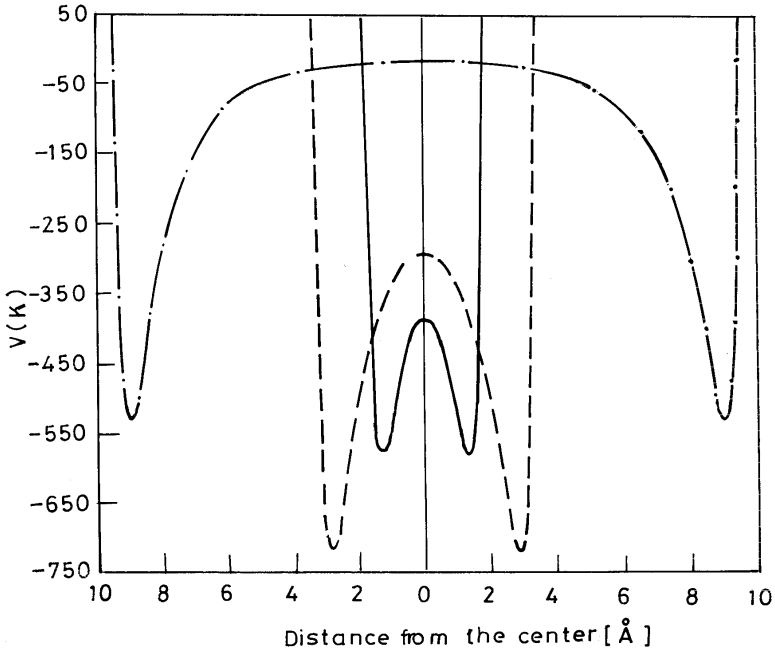

Figure 10.22 Adsorption potentials for hydrogen in tube arrays and idealized split pores. The solid line denotes the idealized carbon split pore with a pore width of 9 Å. The dashed line is the potential for a (9,9) tube array, and the dot-dashed line represents a (18,18) tube array. [Reproduced from Ref. 103]

molecule. The ratio of hydrogen adsorbed in the tube to that on a flat surface decreases strongly with increasing temperature and is 10,000 at 50 K and 100 at 77 K.

6. Most of these simulations do not confirm the high hydrogen uptake capacity obtained experimentally for similar systems of SWNTs and graphitic nanofibers. However, Williams et al reported the results of Monte Carlo simulations for the physisorption of H_2 in finite-diameter 'ropes' of parallel SWNTs (considering the importance of outer surface of ropes), which is consistent with the experimental results obtained by Ye et al at 77 K. Their results show that the maximum gravimetric adsorption capacity of hydrogen onto an isolated (10, 10) nanotube can reach 9.6 wt% under cryogenic temperatures (77 K) and a pressure of 10 MPa. Although their results cannot yet explain the hydrogen adsorption at room temperature, it provides scientists with the confidence to narrow the discrepancy between observed hydrogen storage capacities in SWNTs and the rather large body of data simulation of physisorption.[99]
7. Zuttel et al[103] have presented a model where condensation of hydrogen as a monolayer at the surface of nanotubes as well as bulk condensation in the cavity of the tube was assumed. The potential amount of hydrogen absorbed was calculated to be 3.3 mass% for the adsorption of a monolayer hydrogen at the surface. The condensation of hydrogen in the cavity of the tube leads to a potential absorption for single wall nanotubes starting

at 1.5 mass% and increasing with the diameter of the tubes. Single wall nanotubes with a diameter of 2.2 nm have the potential to absorb 5 mass% of hydrogen. This model suffers from the assumption that the hydrogen condenses in the nanotubes although the critical temperature of hydrogen is 33 K. Gas phase experiments have shown a maximum hydrogen absorption of 0.6 mass% at 78 K for a single wall nanotube sample.

The reversibility of the hydrogen absorption was shown by means of electrochemical absorption/desorption experiments. A maximum desorption capacity of 0.9 mass% was reached for single wall carbon nanotube samples at room temperature. The electrochemically measured discharge capacity at room temperature ($T = 293$ K) of the nanotube samples was correlated with the BET specific surface area. The slope of the linear relationship was found to be 1.5 mass%/1,000 $m^2\,g^{-1}$. Therefore, the extrapolated maximum discharge capacity of a carbon sample was 2 mass%. Furthermore, it was proposed that the hydrogen sorption mechanism was related to the surface of the sample, that is, a surface adsorption process.

Figure 10.23 shows the volumetric hydrogen density versus the gravimetric hydrogen density in various materials. The volumetric density of hydrogen in metal hydrides reaches approximately double the density of liquid hydrogen because the hydrogen intercalates in its atom state in the

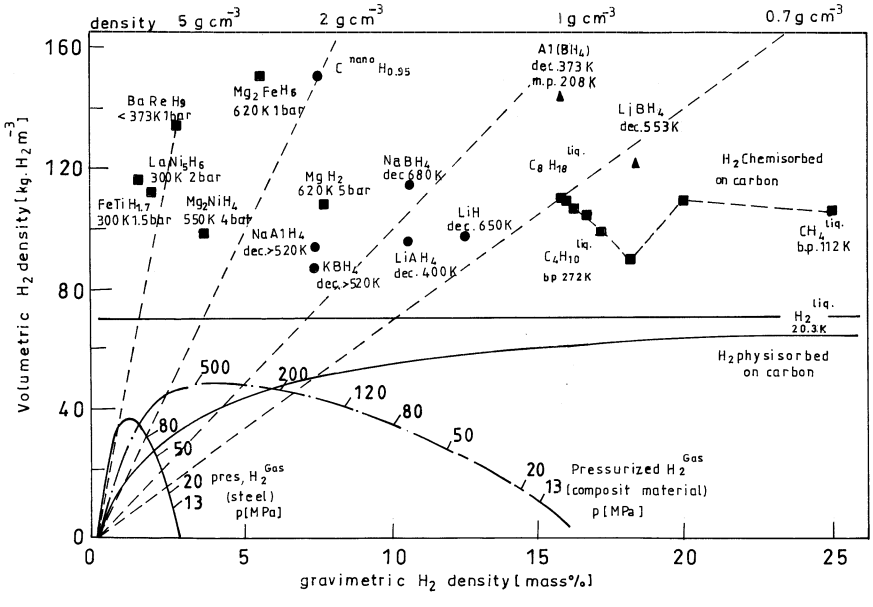

Figure 10.23 Volumetric and gravimetric hydrogen density of some selected hydrides: Mg_2FeH_6 shows the highest known volumetric hydrogen density of 150 kg m^{-3}, which is more than double that of liquid hydrogen; $BaReH_9$ has the largest H/M ratio of 4.5, that is, 4.5 hydrogen atoms per metal atom; $LiBH_4$ exhibits the highest gravimetric hydrogen density of 18 mass%. Pressurized gas storage is shown for steel (tensile strength $\sigma_v = 460$ MPa, density 6,500 kg m^{-3}) and a hypothetical composite material ($\sigma_v = 1{,}500$ MPa, density 3,000 kg m^{-3}). [Reproduced from Ref. 103]

host metal and acts like a metal atom in the host lattice. According to the Westlake criteria,[104] the hydrogen atoms in metal hydrides have an interatomic distance of at least 0.21 nm. This corresponds to an atomic volume of 0.00485 nm^3 and a maximum volumetric density of 187 kg m^{-3}. The volumetric density of hydrogen in hydrocarbons reaches 100–110 kg m^{-3}. The line for nanotubes is universal, that is, all types of nanotubes are on this line as long as the hydrogen adsorption mechanism discussed is correct. Therefore, the only way to increase the volumetric hydrogen density above the density of liquid hydrogen is the dissociation of hydrogen molecules in combination with a tight binding (covalent) or an electron transfer to the host material as in metal hydrides.

It is quite difficult to reach a common conclusion for maximum adsorption capacity and explain the experimental observations from the results obtained by the different theoretical calculations and predictions, though information obtained from the calculations will be helpful for experimental investigation. Meanwhile, clear understanding on the influence of pore structure on the adsorption process of carbon nanotubes will help one to choose the optimum intermolecular potential function and to modify the calculations to direct the development of carbon nanotube-based hydrogen storage systems.

In conclusion of simulation studies, it is established that: (1) at room temperature, opened carbon nanomaterials in a hexagonal arrangement exhibit higher hydrogen adsorption rates than any other carbon materials; (2) gas adsorption efficiency in opened SWNT depends on the nanotube diameters and the distance between the tubes and (3) at low temperatures, high gas adsorption rates needed for practical processes are reached.

10.5.4 Experimental investigations of hydrogen uptake in carbon nanotubes

Most of the current experimental results of hydrogen storage in carbon nanotubes are summarized in Table. 10.6.

Measurement of hydrogen storage

The adsorption is expressed as a unit of quantity of gas with respect to a unit of quantity of adsorbent; the corresponding units are: mole per gram (mole g^{-1}) or gram per gram (g g^{-1}) or, weight % (wt%), which is the commonly used unit now. Rarely is it expressed in atom/atom, that is, atom of hydrogen per atom of carbon.

Three different techniques are mainly applied to study hydrogen storage in solids. The *volumetric method* measures the pressure drop owing to hydrogen absorption after applying a hydrogen pressure to the specimen contained in a constant volume.[105,106] Similarly, the pressure increase due to desorption can be measured. For accuracy and reliable results, this method requires typically, specimen masses of 500 mg or higher. Furthermore, any leakage or temperature instability of the apparatus may give rise to large experimental errors. The advantage of this technique is that both, absorption and desorption can be measured and that the conditions are similar to usage in a storage tank.

The *gravimetric method* measures the weight changes of the specimen due to absorption or desorption of hydrogen. In specially designed devices, a high accuracy can be achieved even

Table 10.6 Summary of cited results

Adsorbent	Hydrogen Storage (wt%)	Conditions Temperature (K) / Pressure (MPa)	References
SWNT(low purity)	5–10	273/0.04	27
SWNT(high purity)	3.5–4.5	298/0.04	
SWNT(high purity)	8	80/8	113
SWNT(50% purity)	4	300/12	114
SWNT	2	80/10	102
SWNT	11	80/10	125
SWNT	~ 0.1	300–520/0.1	137, 138
SWNT (50%–70% purity, electro-chemical)	~ 2	-	80, 141
SWNT	6.5	300/16	142
SWNT	10	300/0.04	111
Li-doped MWNT	20	200–400/0.1	126
K-doped MWNT	14	300/0.1	
Li-doped MWNT	2.5	200–400/0.1	127
K-doped MWNT	1.8	$< 313/0.1$	
MWNT	5	300/10	124
MWNTs (electro-chemical)	< 1	-	139
MWNT	0.25	300/0.1	143
K-doped MWNT	1.8	300/0.1	128
GNFs (tubular)	11.26	298/11.35	129, 130
GNFs (herring bone)	67.55	298/11.35	
CNFs	~ 10	300/10.1	105
CNFs	~ 5	300/10.1	120
GNFs	10	300/8–12	127
GNFs	10	300/12	133
GNFs	6.5	300/12	132
Nano-structured graphite	7.4	$\sim 300/1.0$	140

at sample masses of 10 mg.[107,108] However, this technique is sensitive to all gases absorbed or desorbed since it is only based on weighing.

Thermal desorption spectroscopy (TDS) measures only the hydrogen desorption in high vacuum utilizing mass spectrometry. Moreover, the method is selective and sensitive, allowing to study samples with masses even below 1 mg.[27,109] The sensitivity and selectivity can be even improved by using deuterium loaded specimens.[109] In this case no disturbing background from water or other hydrogen containing adsorbents occurs.

Single-walled nanotubes (SWNT)

Dillon et al[27] were the first to publish experimental data on hydrogen adsorption in nanotubes and measured exactly the desorption of hydrogen of non-purified SWNT samples containing in addition, catalyst (cobalt) and amorphous carbon. Their experimental procedure, Temperature Programmed Desorption (TPD), consists in measuring with a mass spectrometer, the hydrogen desorbed by the carbon sample during a heating run. The sample previously heated under vacuum is exposed to hydrogen at room temperature under a pressure of 300 Torr and then cooled to 133 K. The chamber was evacuated with concurrent cooling of the sample to 90 K prior to the TPD which, in fact, consists in plotting the mass signal of hydrogen on the spectrometer while continuously heating the sample upto 450 K. The authors observed a desorption peak near 150 K and a second peak of less importance near 300 K when their samples were heated upto 970 K before hydrogen exposure. From the amount of hydrogen adsorbed in this second peak and from a graphical integration method applied to the TEM micrograph of the sample, the authors evaluated, at room temperature, a gravimetric storage density for SWNT from 5% to 10% (being 2.5–5 times the maximum stacking of hydrogen molecules into the nanotubes). They also optimized the nanotube diameter for a maximum adsorption to 2 nm, a value for which they claimed that, under the same volume and mass conditions, the energy storage capacity of nanotubes full of hydrogen molecules could be equivalent to the one of a standard reservoir of a petrol automobile, a pleasant and optimistic conclusion! They have showed that hydrogen can condense to a high density range (estimated to $5 \sim 10$ wt%) inside narrow SWNTs of 12 Å, and predicted that SWNTs with diameters of 16.3 and 20 Å would come close to the target H_2 uptake density of 6.5 wt%. These experiments suggested that physical adsorption of hydrogen mainly occurred within the cavities of SWNTs. The activation energy for hydrogen desorption was found to be 19.6 kJ/mol, which is higher than the theoretically predicted value discussed previously, or approximately five times higher than that for a planar graphite surface, thereby promoting hydrogen storage capacity at higher temperature.

In a more recent paper, Dillon et al[111] presented an oxidative technique to open the nanotubes: the degassing of the samples in vacuum to 970 K and oxidizing in water in the 325–975 K temperature range. They have measured the adsorption of hydrogen in such treated samples by the TPD method and found a noticeable enhancement (upto a factor of three in the most favourable case) of the habitual peak of desorption between 250 and 300 K. They attributed this improvement of the adsorption capacity to the opening and filling of the nanotubes. Taking into account that their carbon soot samples containing only 0.05% of nanotubes can adsorb $\sim$ 0.005% weight of hydrogen, Dillon and his colleagues concluded that the pure adsorbed hydrogen is therefore $\sim$ 10 wt%.

Lamari et al[112] have investigated the amount of hydrogen stored in a tank-full of activated carbon for different gas thermodynamic conditions. The analysis of the thermal exchange dynamics during the charge operation was investigated through the modelling of the coupled energy and mass transport that takes place in the reservoir. They obtained a maximal temperature elevation of about 30 K inside the tank when the charge of the gas was under a pressure of 15 MPa. The efficiency in this case was about 85% during the reservoir charge procedure. Indeed, the model used was validated by experimental measurements carried out on different adsorbents such as activated carbons. It would be interesting, on the one hand, to predict the thermal effects that could occur in

a hydrogen gas reservoir full of carbon nanotubes and, on the other hand, to evaluate the efficiency of storage of these adsorbent materials.

Ye et al[113] measured the hydrogen adsorption on SWNT samples which they prepared and purified. With the aim of cutting the tubes and disrupting the rope structure, their samples were sonicated in a solution of dimethyl formamide until the carbon was completely suspended in the liquid. The nanotubes were then extracted by vacuum filtration through a ceramic filter. High-resolution transmission electron micrographs of this sonicated material show that ropes with diameters ranging from 6 to 12 nm, are comparable to those of untreated material but with broader size distribution and more irregular patchwork of fringes caused by more terminations of individual SWNT within the ropes. After a 10 h degassing run at 220 °C, the adsorption of hydrogen was measured by a volumetric method with a Sieverts apparatus which measures pressure variations due to the adsorption or desorption. It is regrettable that corrections of thermal effects resulting from the compression–decompression of the gas and from the adsorption–desorption were not given. Measurements have been carried out at room temperature, 300 K, at a pressure of 160 bar and also at low temperature, 80 K, at pressures of 130, 70, 4.5 and 0.5 bar.

The authors did not present explicitly their results of adsorption at room temperature but only noted that this adsorption is proportional to the BET surface of 285 m^2 g^{-1}, which they have determined, taking as reference the adsorption—not given—of Saran carbon having a BET surface of 1,600 m^2 g^{-1}. In an indirect way, it is reported that in ambient conditions, the adsorption of hydrogen in carbon nanotubes is 18% of that in current activated carbon. At 80 K, Ye and his colleagues presented the results of several adsorption runs: the first one on a fresh sample which exhibits higher adsorption values, upto 1 atom/atom at 60 bar; while the second and subsequent runs correspond to high-pressure adsorption values reduced by half. The explanation proposed is that the first adsorption–desorption cycle reorganizes the tubular structure in a more perfect triangular lattice, causing subsequent low adsorption at high pressure. As concerns sonification, the reduction of cohesive energy of the rope structure leads to an increase by a factor of two of the adsorption under a pressure of 60 bar. To summarize, the values of hydrogen adsorption on hydrogen measured by Ye et al[113] at 80 K is of the order of 0.5 atom/atom in the range 40–80 bar, whatever may be the adsorption desorption run with a sample-sonicated or not. Compared to the adsorption of Saran carbon, the situation at low temperature is unexpected: the adsorption of carbon is higher than the one of nanotubes upto 30 bar; at higher pressures the adsorption isotherm of nanotubes increases almost linearly whereas the Saran carbon isotherm leads to saturation at a pressure of about 100 bar. This particular behaviour is probably due to the fact that, because of their difference of structure, the accessibility of adsorption sites is easier for Saran carbon than for nanotubes, as it is confirmed by the relatively rapid saturation of the carbon. At room temperature it can be supposed that the situation is the same, but the intersection and the saturation of isotherms take place at higher pressure in a range not investigated upto date. In their conclusion, the authors stated that the ability of SWNT material to adsorb and desorb hydrogen over a narrower range of pressure may be used in storage systems without wide pressure excursions.

Liu et al[114] determined the adsorption of hydrogen on SWNT having a purity of 50%–60% which they have synthesized by a semi-continuous hydrogen arc discharge technique. They also treated their samples by hydrochloric acid and vacuum heated at high temperature, and compared the corresponding incidence of these purifying treatments. Their adsorption measurement technique

consists in monitoring time versus the pressure change of hydrogen introduced in a constant-volume cell containing the nanotubes sample; when the equilibrium is achieved, the total decrease of pressure corresponds to the amount of hydrogen adsorbed. The results are, respectively, 2%, 2.5% and 4% weight for non-treated, partially treated and entirely treated samples. As concerns the two thermal effects resulting from the hydrogen filling of the sample cell, they have apparently not been taken into account. One of these effects is due to the gas compression upto the target filling pressure, 10–12 MPa; the second is due to the gas adsorption during this filling. The two thermal contributions being exothermic, they contribute to increase the gas temperature, and then the gas pressure, at the initial time of the pressure change measurements, with the consequence of overestimating the amount of hydrogen adsorbed. As in the case of the above-cited paper of Ye et al,[113] in the absence of an evaluation of this effect (probably low) and of the incidence in the adsorption measurement value, the present adsorption capacity data are partially reliable.

Nützenadel et al[80,115] investigated the hydrogen sorption properties of nanotubes at room temperature (298 K) in an electrochemical system and found a maximum desorption (electrochemical discharge) capacity of 0.41 mass% with an SWNT sample obtained from Materials & Electrochemical Research (MER) Corporation of Tucson, Arizona, USA. Later on, Nützenadel et al[116] measured an electrochemical low current discharge upto 2 mass% on purified SWNT samples.

Dillon et al[117] reported recently the experiments on purified (ultrasonically pre-treated) SWNTs which were exposed to 50 kPa hydrogen gas at room temperature. Subsequently, the sample was investigated by means of temperature programmed desorption spectroscopy (TPD). The spectrum shows a double peak—the major peak at 620 K and the minor at 350 K. The amount of desorbed hydrogen was 6.5 mass% determined from a comparison with the desorption peak found for CaH_2. The peak position in this work is quite different from the peak positions given in the previous paper.[27] Furthermore, Hirscher et al[118] investigated the influence of an intense ultrasonic treatment on SWNTs using a Ti-alloy bar in 5 M HNO_3, the same method that was applied by Dillon et al.[117] This procedure was applied to SWNTs in order to open the caps of the nanotubes and make the cavity accessible for the hydrogen gas. The authors have shown that the treatment leads to an incorporation of Ti particles in the sample as a function of the duration of sonication. The majority of hydrogen storage was ascribed to the metal particles.

Liu et al have developed a semi-continuous hydrogen arc discharge method to prepare SWNTs on a large-scale.[119] Both HRTEM observations and resonant Raman measurements proved the existence of larger diameter SWNTs (1.6 $\sim$ 2.0 nm).[119–121] High-resolution adsorption measurements showed that the sample has abundant micropores of diameter similar to tube diameter, indicating much more open tubes.[122] According to Dillon's[27] and Cheng's[123] predictions, this kind of SWNT may be promising as high hydrogen storage carriers. Figure 10.24[114] shows the change of hydrogen pressures as a function of time for SWNTs under an initial hydrogen pressure of 10 MPa in the first adsorption cycle at room temperature. The hydrogen uptake is complete within a few hours. It was shown that even assynthesized SWNTs have hydrogen uptake capacity,[114] possibly resulting from the open tubes in the sample. Meanwhile, it has been proved that notable changes occur for pore structure in the course of hydrogen uptake in SWNTs. All the above facts indicate that the inner hollow cavity takes part in the hydrogen adsorption. In the previous section, it was emphasized that interstitial adsorption constitutes a significant fraction of the total amount

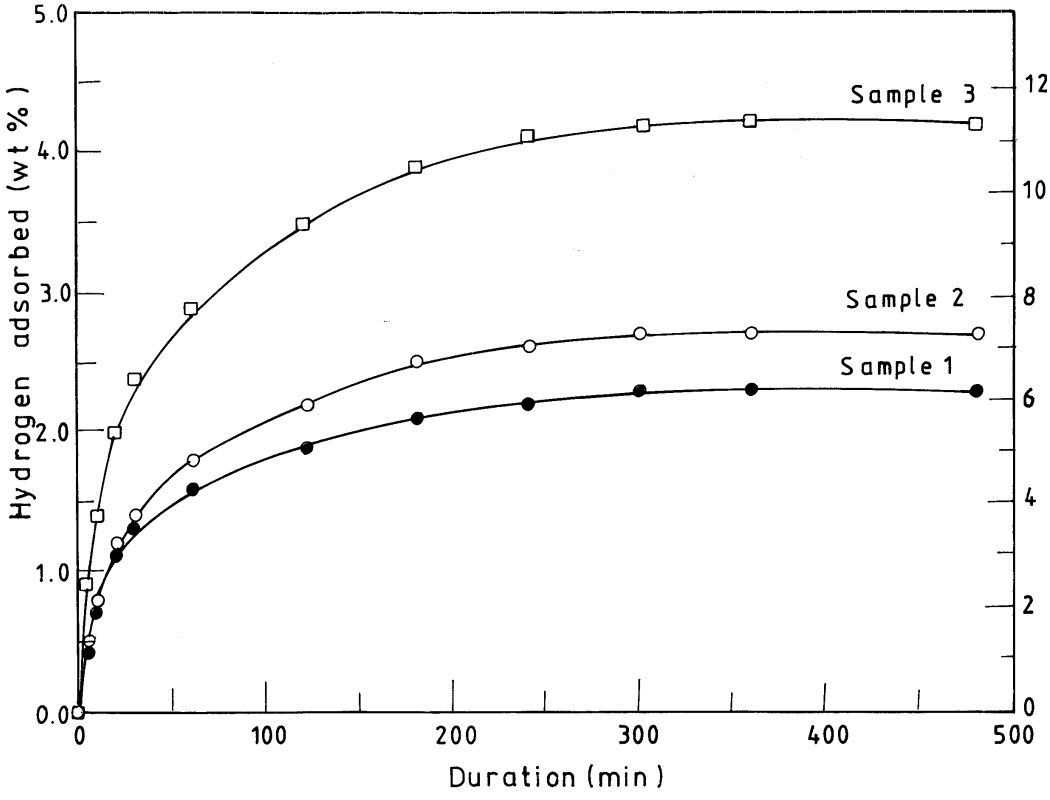

Figure 10.24 The amount of H_2 in weight for SWNT samples, and the pressure change vs the adsorption time: Sample 1 was used as synthesized; Sample 2 was soaked in 37% HCI acid for 48 h, rinsed with deionized water, and dried at 423 K; Sample 3 was pretreated in the same way as sample 2, then vacuum heat-treated for 2 h at 773 K. [Reproduced from Ref. 114]

adsorbed for larger diameter tube arrays, thus, for this kind of SWNTs with large diameter (about 1.8 nm), a fraction of the adsorbed hydrogen may fill the inter-tube spacing. In other words, it is more open tubes (providing inner surface) with large diameters (making the interstitial space accessible) that lead to the high hydrogen adsorption capacity.

Multi-walled carbon nanotubes (MWNT)

The adsorption property of this type of nanotubes has been recently studied. Zhu and his collaborators[124] obtained their samples by catalytic decomposition at 900 °C of an acetylene–hydrogen mixture, submitted to successive treatments after it was milled with a ball grinder to break larger tubes: (1) attacked by nitric acid; (2) immersed in an alkali (NaOH) solution and after drying, submitted to a calcination at 823 K; (3) heated for 2 h in an argon environment under high temperature, (800 °C), and very high temperature, (1,700 °C). The nitric acid treatment eliminates

impurities and contributes to open caps of some tubes but it greatly increases the number of surface oxygen functions (discovered in XPS spectra) which weaken the adsorption capacity of the nanotubes. NaOH is an excellent dispersing agent; it avoids the agglomeration of nanotubes and then increases the surface area. As concerns the high-temperature treatment, especially at 1,700 °C most functional groups are removed (observed by infrared spectroscopy). The respective effects of these treatments on the adsorption capacity of hydrogen at room temperature and 100 atm are: 2.67% for sample (1); 4.12% for sample (2); 2.5% and 5.08% for heated samples (3). It must be noted that the authors did not give explicit details on their measurement procedure or provide accessible reference giving a description; they merely presented a schematic diagram without explanation. It is possible to assume that they have used a constant volume method based upon the measurement of the pressure. For such a measurement technique being comparable to those cited above, a reserve on the reliability of the results has to be made even if the thermal effect contributions were to be low.

Zhu et al[124] have explained the hydrogen adsorption in their carbon nanotube samples as a concomitant process of both physical and chemical adsorption, but they did not mention what the exact part of the two phenomena is, neither in the adsorption mechanism description nor in the measured quantities. They only explained that the aim of the surface treatment is not only to remove contamination but also to form micropores or etch grooves on the nanotubes. Through these surface irregularities, and while the adsorbed hydrogen rises above a given concentration, hydrogen molecules diffuse into the nanotube layers, the consequence being a strong interaction with delocalized π electrons of the basal graphite plane.

Wu et al[125] have obtained multi-walled carbon nanotubes from the catalytic decomposition of CO and CH_4 on powder Co/La_2O_3 catalyst. They found that by adjusting the composition of the catalysts, the size of the nanotubes was controllable, and by annealing, the crystallinity could be improved. They concluded that their nanotubes are 'able to uptake a certain amount of H_2 under ambient conditions'.

Alkali-doped carbon nanotubes

In 1999, Chen et al[126] have published the data on the hydrogen storage capacity of nanotubes doped with Li and K. They prepared their samples by catalytic decomposition of CH_4. After purification, almost all the catalyst particles were removed and the product was in the form of MWNT in a diameter range of 25–35 nm. The doping of Li and K was carried out by solid state reactions between CNT and Li- or K-containing compounds such as carbonates or nitrates. The Li/C and K/C ratios were about 1/15, as measured by X-ray photoelectron spectroscopy. Hydrogen uptake was measured by thermogravimetric analysis. Samples were initially heated in situ at 873 K in a flow of purified hydrogen to remove adsorbed water and contaminants. The Li-doped samples were cooled to 300 K and heated again to 873 K. The nanotubes so doped adsorbed, 20 wt% and 14 wt% of hydrogen at 1 atm and a temperature of 200–400 °C for lithium doping and for potassium doping respectively.

Some months later, Yang[127] revisited these data. He prepared the doped nanotubes following the same procedure and also measured the adsorption–desorption using a comparable thermogravimetric analyzer. His conclusion is that special caution needs to be taken to remove any moisture contamination of the hydrogen in measuring the adsorption. Moisture drastically increased the

weight gain picked up and this put the results in error. So, in dry hydrogen, the adsorption is of 2.5 wt% for lithium-doped nanotubes and of 1.8% for potassium-doped nanotubes, as per results more recently confirmed by Pinkerton et al.[128]

Other carbon nanostructures

Single- and multi-walled nanotubes are not the only carbon structures which are able to retain hydrogen in their framework. Graphite nanofibers (GNF) studied by Rodriguez and her colleagues[129,130] also exhibit hydrogen adsorption properties. These fibers are produced from the dissociation of carbon-containing gases over selected metal surfaces and consist of very small graphite platelets 3–50 nm in width that are stacked in a perfectly arranged conformation. The authors claimed that this material, exposed to 120 atm of hydrogen at room temperature, is capable of sorbing and retaining in excess upto 23 l (STP) of this gas per gram of carbon—65.55 wt%—a value that is over an order of magnitude higher than that was found with conventional hydrogen storage systems! Later, the same team confirmed their results with more detailed explanations of such an important hydrogen molecule intercalation between the graphene sheets of the nanofibers.[130] Unfortunately, to date, this hydrogen adsorption amount—capable of solving the hydrogen storage problem—has not been confirmed, neither experimentally nor theoretically.

They have claimed that tubular, platelet and herringbone forms of GNFs were capable of adsorbing in excess of 11, 45, and 67 wt% H_2, respectively, at room temperature, under a pressure of about 12 MPa. Their later paper[131] reports further results on the interaction of hydrogen with GNFs, and proposed that the GNFs possess special structural conformation, which produces a material composed entirely of nanopores that accommodate small-sized adsorbate molecules such as hydrogen, and the non-rigid pore walls can expand to accommodate hydrogen molecules in a multilayer conformation. They also pointed out that the pretreatment before hydrogen storage is very important and that ambient humidity is deadly harmful to the hydrogen uptake performance.

Browning et al[132] synthesized carbon nanofibers at 600 °C by passing ethylene over a series of Fe/Ni/Cu catalysts. They have obtained a hydrogen storage in their sample at room temperature and 120 atm of 4.18 wt% and 6.54 wt%, respectively, with a post-production treatment. Gupta et al[133] also measured the hydrogen adsorption capacity of several carbon nanostructures—nanotubes, Li- and K-doped nanotubes and graphite nanofibers—they elaborated by the methods which now are well known. They found that the best results were obtained on graphite nanofibers: 10 wt% at 120 atm and 27 °C.

Nanostructured graphite was investigated by Orimo et al[134] for hydrogen absorption and desorption. Graphite was ball milled for a maximum of 80 h in a 1 MPa hydrogen atmosphere. The hydrogen absorbed in the sample was determined by means of oxygen-combustion hydrogen analysis and it turned out to be as high as 7.4 mass% (C/H = 0.95). This result shows that high hydrogen absorption can also be realized without the hollow structures of nanotubes.

A large variety of carbon samples was investigated, using a high pressure micro-balance, by Ströbel et al.[107] The BET (N_2) surface area of the samples ranges from 100 m^2 g^{-1} upto 3,300 m^2 g^{-1}. The absorbed amount of hydrogen (p = 12.5 MPa, T = 296 K) correlates with the surface area according to the equation x (mass%) = $0.0005S$ (where S is surface area in m^2 g^{-1}) except for the nanofiber samples. The latter exhibits a rather low surface area of

approximately 100 m^2 g^{-1}; however, the increase in mass upon hydrogen absorption corresponds to about 1.2 mass%. The adsorption isotherms measured follow approximately the Langmuir adsorption model. Some isotherms intercept the mass-axis ($p = 0$) at $x = 0$, others intercept at a finite mass between 0.2 and 0.4 mass%.

Fan et al[105] investigated the hydrogen absorption of vapour-grown carbon nanofibers (CNFs) with a diameter of 5–300 nm. The fibers absorbed hydrogen upto 12.38 mass% when a hydrogen pressure of 12 MPa was applied. The absorption was equilibrated in 200–300 min. They have observed that CNFs of 100 nm diameter possess high hydrogen storage capacity ($5 \sim 10$ wt%) at room temperature under moderate pressures.[105,120] Recently, their experimental results showed that MWNTs ($3 \sim 20$ nm diameter) also have a high gravimetric hydrogen storage capacity. The various post-treatment methods seem to modify the pore structure and surface microstructure and consequently, enhance the hydrogen adsorption capacity to a considerable extent. In conclusion, pore structure and surface microstructure exert a large influence on the hydrogen storage performance of CNFs, MWNTs and SWNTs.

The hydrogen storage capacity of carbon nanotubes and nanofibers is determined by physical properties such as pore geometry, surface area and appearance of graphene sheets, which are influenced by the synthetic methods. Catalytic decomposition or pyrolysis methods with hydrocarbon—among the several ways to produce carbon nanotubes or nanofibers—are widely used because of easy synthesis, controlable size and purification of the nanotubes. In addition, to enhance the capacity of hydrogen uptake in carbon materials, various processes are applied not only for appropriate storing means but also for handling physical properties like doping and surface treatment with carbon materials.[88]

For instance, Hwang et al[89] have prepared carbon nanofibers having herringbone structure with hollow cylindrical shape and open ends as well as short length (it was hypothetically considered as suitable for hydrogen storage due to pore geometry) and surface treatment was carried out to enhance hydrogen adsorption capacity. Ni–MgO catalyst and CH_4 were used for synthesis of nanofibers by thermal decompostion. Subsequently, hydrogen uptake capacity was measured by a Sieverts' apparatus. The outer diameter of tubule-like carbon nanofibers range from 20 to 40 nm and the hollow inner diameter covers about 5–10 nm. The length of the fibers was shorter than those made by arc-discharge or laser vapourization, hence, the edges also appeared at the end of the nanofibers. The carbon nanofibers typically have a hollow centre and herringbone type graphite layers at an angle with respect to the fiber axis, and consisting of two kinds of ends: one open and the other closed. The maximum capacity of saturated hydrogen uptake in these samples is 1.4 wt% in the case of the heat treated sample which exceeded the non-annealed sample by 30 wt%. Similar trend was also previously reported for single-walled carbon nanotubes.[114]

The first hypothetical assumption was change of interlayer distance (d-value) after heat treatment. The interlayer distance of the (0 0 2) plane known as a site for hydrogen[129,130] was increased approximately 0.6%, from 0.340 to 0.342 nm, after heat treatment in this case. However, this is negligible because at the value of the interlayer distance, no hydrogen can be adsorbed, as reported by Rzepka et al.[100] Their theoretical and experimental approach intimated that although the d-value is expanded to 0.7 nm during the adsorption process, the excess hydrogen uptake is under 1 wt%. Moreover, heat treatment over 2,000 °C of CNFs will increase the crystallinity; so the graphene layer's distance will be closer. Thereafter, heat treatment is rather a disadvantage if

the interlayer distance has an important role in hydrogen uptake, as referred by Rodriguez and coworker.[129,130]

Secondly, Liu et al[114] indicated that annealing, performed in vacuum for 2 h at 500 °C, could evaporate organic compounds and impurities on the surface of carbon nanotubes formed during the synthetic procedure and acid treatment. Interestingly, it was shown that thermal activation of single-walled carbon nanotubes over 600 K, enhanced the adsorption capacity for Xe at 95 K[90] and showed a similar trend with the case of Hwang et al.[89] It was ascribed to the removal of a large number of functional groups, which would offer entry ports for adsorption on the inner surface of the nanotubes. Gas chromatographic analysis confirmed this concept. At about 800 °C, carbon dioxide and carbon monoxide were evolved from CNFs. As the temperature was increased to 1,200 °C, CO_2 and CO mole fraction was also increased. After heat treatment at 1,200 °C for 2 h, the total weight loss of CNFs was 30% compared to that before heat treatment. It was therefore supposed precariously that the increment of hydrogen uptake after heat treatment at 1,200 °C was due to augmenting of disordered surface structure. Under 1,200 °C, oxidation process occurs more actively on surface in the presence of O_2 and H_2O rather than graphitization of CNFs, so the outer wall after annealing has rough and defected graphene layers more than before heat treatment, which may induce the specific surface area increase for the hydrogen adsorption site. It was evident that the surface area measured by BET has been increased from 140 to 170 m^2 /g.

10.6 Critical Analysis of the Reported Results

The various reported results on hydrogen storage in carbon nanomaterials are summarized in Table 10.6.

Let us discuss three gravimetric storage benchmarks.

1. 0.7 wt% experimental for activated carbon and calculated for an ideal slit pore with a specific surface of 2,600 m^2 /g at $T = 300$ K and $p = 6$ MPa.[18] The atomic ratio H/C = 0.085 means that 1 hydrogen atom is assigned to 11.8 atoms of carbon on an average and 1 H_2 is assigned to 23.6 C.
2. 6.5 wt% is the US Department of Energy (DOE) benchmark of system weight efficiency.[88,27] The atomic ratio H/C is 0.83; this means that 1 H atom is assigned to 1.2 C atoms.
3. 67.5 wt% is the maximum value for storage in herringbone fibers.[129,130] The atomic ratio H/C is 25. This means that 25 H atoms are assigned to 1 C atom.

The DOE benchmark requires almost one hydrogen atom per carbon atom. This is similar to the C_2H_2 molecule, which has strong covalent bonding. Such a ratio for H_2 gas and a pore pattern seems to be unrealistic for capillary forces built on van der Waals' interactions. In the last case, 25 hydrogen atoms are assigned to one carbon atom. Carbon is diluted in hydrogen, a reversal of what one would expect! This basic calculation of the atomic H/C ratio gives us a guide for a reasonable storage limit.

Promising publications reporting high hydrogen storage capacities in carbon nanotubes resulted in enormous research activity, yielding much experimental data. These data, however, exhibit a large scatter, as exemplified for single-walled carbon nanotubes (SWNTs) in Fig. 10.25. For

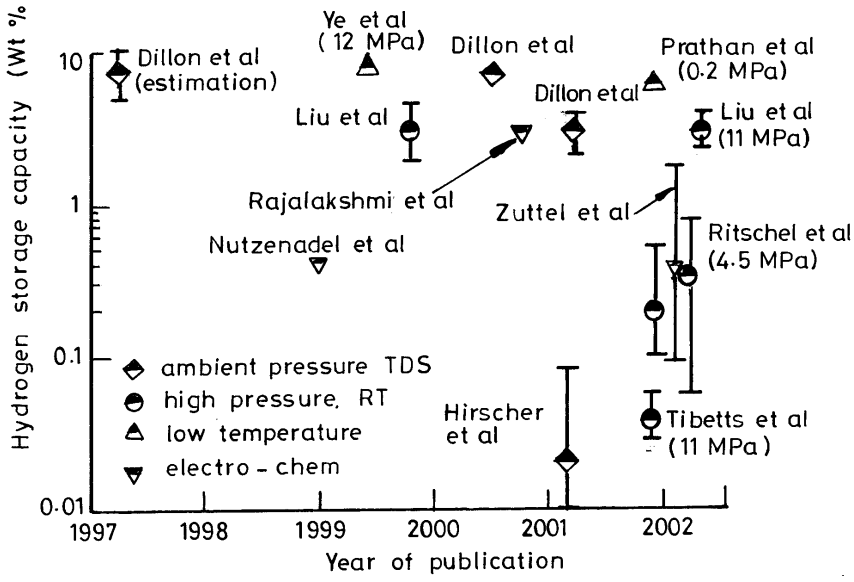

Figure 10.25 Experimental data for hydrogen storage capacities (logarithmic scale) in SWNTs versus publication year for different methods, pressures and temperature regimes

graphitic nanofibers, the results are even more scattered, and storage capacities from 67 down to 0.1 wt% have been reported. However, the extremely high storage capacities have never been independently reproduced in another laboratory. Considering the experimental results for metal hydrides, the storage capacities of which have been reported to vary only within a few percent since their discovery many years ago, why is it so difficult to determine the hydrogen storage capacity of carbon nanostructures? One reason may be the limited quantity and purity of carbon nanotubes. Furthermore, a reliable characterisation of carbon nanostructures and the determination of their purity is extremely difficult. But can these difficulties really explain the extreme discrepancies between different research groups?

Among these data, it appears that, except for those of Chambers et al[129] at room temperature, the hydrogen uptake is of the order of a few percent, a value also obtained by Ye et al[113] at 80 K. The latter experimental value is compared to the one computed by Darkrim et al[122] by molecular simulations with comparable thermodynamic conditions and for nearly the same SWNT configurations as those described by Ye et al.[113] The results given in Table 10.1 correspond to a range of pressures between 0.04 and 12 MPa, a proof of their scattering since pressure is the main parameter of variation in adsorption along an isotherm of adsorption. This is probably due to the relative difference in the nature and in the composition of the samples but it is also due to the fact that measurements were performed with a small amount of sample material on sensitive apparatus for several hours. During such a long time of measurement, the physical stability has to be maintained to avoid drifts of devices. Finally, because of some experiment sequences carried out at high temperatures—in particular, contact of samples with hydrogen and desorption—the extent of physisorption and chemisorption should be exactly identified, a reason why the authors carefully

use the word 'uptake'. So, the question is: can these 'uptakes' of hydrogen be applied to storage on board a vehicle? Especially if, in addition, one considers the short time required to absorb and desorb hydrogen as suggested in the works of Lamari et al?[112] They have studied theoretically and experimentally the thermal effects in dynamic hydrogen storage by adsorption at room temperature and high pressure. The theoretical analysis was based on heat- and mass-transfer modelling in a packed-bed adsorber, with particular emphasis on the thermal effects occurring during the charge and discharge steps. The influence of gas flow rate and storage pressure (upto 15 MPa) on the total amount stored or delivered was investigated. Operating conditions were compatible with practical application for on-board vehicle storage.

There exists an uncertainty about the accessibility of nanotubes to hydrogen molecules for two main reasons: (1) when they are open, their diameters are of the order of molecular size and their lengths three orders higher; (2) the space between tubes in the bundles has the same, high length/diameter ratio.

It is important to notice that different factors can influence the gas adsorption. Among these factors, we can cite the specific area of the materials, the method used in order to open the tubes, the intercalation of heteroatoms in order to increase the gas uptake and the purification of the adsorbent,[143] before any adsorption measurements are done. Gas adsorption is dependent on the specific area of the material. In the case of the nanotubes, some values have been published: they vary from 200 to 800 $m^2\ g^{-1}$. This material property is more or less important, depending on the adsorbent synthesis method employed. Usually, the electric arc method is the one used by Stepanek et al[144,145] and the laser ablation one could lead to 'low' specific surfaces whereas the CVD method seems to give higher values as described by Basca et al.[146] Moreover, there exist different methods to open the tubes, including mechanical and chemical ones. Hiura et al[147] and Ajayan et al[148] used the oxidative procedure to open the extremities of their nanotubes whereas Stepanek et al[145] used the cutting method by abrasion with a diamond disc. Intercalation methods have also been developed to induce chemical gas adsorption with the new atom.[149,150]

It is also important to remark that there seems to be no difference between the hydrogen adsorption phenomenon at room temperature or at low temperature in SWNT, MWNT or GNF materials. Indeed, it is in all the cases, the gas physisorption on graphite surfaces which exhibit different shapes or forms. However, the hydrogen gas interacts in the same way by van der Waals interaction with the carbon atoms constituting the adsorbent nanomaterials. Of course, it is noticeable that at high temperature or in the presence of heteroatoms in the adsorbent (due to the chemical treatments that occur during the material synthesis), the gas–adsorbent interaction will be different from the one described above.

Firstly, one can notice that the treatment of the adsorbent surface (high temperature and vacuum treatments) before any adsorption investigation is carried out, is important in order to achieve high gas adsorption. Moreover, this survey of published results enables us to conclude that gas adsorptive properties are pressure- and temperature-dependent as in the case of any adsorbent material.

Despite the importance of the hydrogen adsorption capacity of nanotubes for a reliable storage, the bulk density of the nanotubes has to be taken into account. Indeed, the amount of hydrogen stored is directly proportional to the adsorption expressed in weight % and consequently, to the bulk

density of the adsorbent. For carbon nanotubes this bulk density is about 20 kgm^{-3} whereas for current carbonaceous adsorbents it is of the order of 500–1,000 kgm^{-3}. Due to the fibrous character of the carbon nanotubes, it was noticed that they can be easily compacted. Carbon nanotubes can be compacted by uni-axial press and without binder. The method of material compaction is described by Darkrim and Malbrunot.[151] The solid material obtained is mechanically stable, with a bulk density of about 800 kgm^{-3}, and their adsorption properties are not especially altered. This mechanical study should be done in purified carbon nanotubes and then one should measure a noticeable gas adsorption amount in clean material. The next step should be the measurement of hydrogen adsorption in purified and opened carbon nanotubes in order to enable gas adsorption, both inside and outside the compacted bundles of carbon nanotubes.

An examination of the actual state-of-the-art of hydrogen adsorption in carbon nanotubes involves the fundamental question: Can adsorption in nanotubes be a reliable mode of hydrogen storage for vehicular application?

The answer is 'perhaps', if one considers the results of the synthesis of SWNT, of their purification processes, of the opening of their ends and of some measurements of adsorption of hydrogen mentioned above. The arc discharge synthesis is now reliable. On the other hand, it must be recognized that the purification is a problem that is difficult to solve and especially so at the level of the yield. The consequence is that the amount of sample obtained is not sufficient to carry out reliable experimentation at room temperature on the adsorption of excess hydrogen, the only quantity which is significant for the evaluation of the storage capacity of an adsorbent. As concerns the opening of the tubes, it is essential to ensure that hydrogen molecules can enter the tube because these molecules cannot penetrate through the carbon atom hexagons. The values of hydrogen adsorption obtained by different authors are relatively scattered, probably due to the small amount of samples which have non-reproducible characteristics. SWNTs have many potential advantages for hydrogen adsorption over currently available adsorbents. They have large theoretical surface areas that are on the order of those for high-surface area activated carbons. Crystallized arrays of SWNTs have a narrow pore size distribution that has virtually all their surface area in the micropore region. In contrast, surface area in activated carbons is broadly distributed between macropores, mesopores and micropores. The pore sizes in an array of tubes could be controlled by tuning the diameter of the SWNTs making up the array. Nevertheless, these adsorption results are sufficiently significant to be of interest.

The answer is 'yes', if one considers data obtained experimentally by several authors. Several Monte Carlo simulation studies also gave values of adsorption of hydrogen in all the cases higher than those given by the better carbonaceous adsorbents. These simulations have also put into evidence that this hydrogen adsorption can be optimized by suitable sizes of nanotube diameters and by space between nanotubes in the bundles, such results being indications for future developments of nanotubes. If one takes into account that Monte Carlo simulations have been performed on pure, well-dimensioned open nanotubes, a definitive answer to the precedent question will be given, when nanotube samples for adsorption experiments will be available in sufficient quantities, with a high degree of purity and containing numerous openings for hydrogen accessibility.

The experimental and computational studies of carbon nanotube adsorption property lead one to conclude that these materials seem to be good candidates for the hydrogen storage process. However, some questions still persist.

In particular, the main concerns are on the surface properties of these adsorbent materials:

- the chemical treatment during or after the carbon nanotubes synthesis;
- the mechanical treatment made on the tubes in order to open their extremities and enable the gas adsorption inside the tubes;
- the amount of reactive nanotubes (attributed to their low purity rate after their synthesis) taken into account in the gas adsorption calculations;
- the presence or not of heteroatoms on their surface which can contribute to modify the electronic density on the nanotube surface, so that the reactivity of the material can be reinforced (for instance, it is possible to intercalate alkali atoms between consecutive tubes);
- the accuracy of the volumetric and the gravimetric measurement methods should be mentioned;
- the definition of the hydrogen 'uptake' used by the authors in their works (excess of adsorption or total amount of the gas).

Once these respective main influencing factors on hydrogen adsorption in carbon nanomaterials are well determined and established, one will be able to predict, explain and validate the various adsorption amounts published in the literature and control one's own adsorption data, which is unfortunately often obtained on one's own characterized materials.

10.7 Perception

Reflecting on the inconsistency in the reported values of hydrogen uptake by carbon nanotubes, one will be tempted to prioritize the steps as follows:

1. Evolution of 'cost-effective' standard method for the mass production of carbon nanotubes,
2. Standardization of the methods for the purification of the materials produced,
3. Formulation of appropriate pretreatment conditions,
4. Elucidation of the texture of the evolved carbon materials in a consistent manner,
5. Examination of storage capacity and storage limits under specified and reproducible conditions,
6. Postulation of mechanistic details of the process on well-focussed basic assumptions,
7. Interpretation of results obtained in a consistent manner with due care to the possible species that can coexist with the formulated carbon materials.

10.8 What is Still Unknown?

In addition to what has been discussed in this chapter so far, it is essential to state what is still unknown in our own perceptions, and these aspects have been already reflected by us some time ago.[152] Brushing aside the foresight on the widening widths of application potential windows and prophesies on outcomes, we concentrate our perceptions on '*what is still unknown*' in the underpinning science on this '*up-taking*' (adsorption-absorption) phenomena.

- Exploitation of carbon materials for hydrogen storage – is it conceptually an extension of Nature's method? If so, are we proceeding in the right direction to exploit this concept originated from nature?
- Have we broadly specifically identified the domains in the variables under which this application has to be exploited?
- Have we understood clearly the adsorption potential and how they are altered in different forms of carbon materials and what is special about carbon nanomaterials?
- Which other forms of carbon still have such properties and why?
- What is the state of the hydrogen atoms in the 'Adsorption State' . . . .have they still maintained their atomic or molecular characteristics?
- And above all, what is the most preferred geometric location for the hydrogen and in what state and why?

In all, hydrogen fuel is clean, versatile, efficient and safe, and is the best fuel for transportation. Hydrogen energy will play an important role in the future world energy scenario. Taking all these results together, we consider it to be scientifically interesting and challenging to continue research on the interaction of hydrogen with different and well-characterized carbon nanostructures. Carbon nanotubes and carbon nanofibers can be promising candidates for hydrogen storage, which may accelerate the development of vehicles driven by hydrogen fuel cells.

References

[1] Dunn S, *Int. J. Hydrogen Energy*, 27:235–264, 2002.

[2] Hefner RA, GHK Company, Oklahoma City, OK, 10th *Repsol-Harvard Seminar on Energy Policy*, Madrid, Spain, 3 June 1999; Ausubel JH, Where is energy going?, *Ind. Phys.*, 16–19, 2000.

[3] King RO, Rand M, The hydrogen engine, *Canad. J. Technol.*, 33:445–469, 1955.

[4] Maxwell TT, Jones JC, Alternative fuels - missions, economics and performance, *SAE*, Warrendale, Mich., USA., 1995.

[5] Appleby AJ, Fuel cells and hydrogen fuel, *Int. J. Hydrogen Energy*, 19:175–180, 1994.

[6] Kukkonen CA, Shelef M, Hydrogen as an alternative fuel: 1993 update, *SAE*, Paper #940766, 1994.

[7] Steinberg M, Cheng HC, Modern and prospective technologies for hydrogen production from fossil fuels, *Int. J. Hydrogen Energy*, 14:797–803, 1989.

[8] Rose JW, Cooper JR, *Technical Data On Fuels*, Scottish Academic Press, Edinburgh, UK, 1977.

[9] Karim GA, *Int. J. Hydrogen Energy*, 28(5):569–577, 2003.

[10] Karim GA, Wierzba I, Al-Alousi Y, Methane-hydrogen mixtures as fuel, *Int. J. Hydrogen Energy*, 21:625–634, 1996.

[11] Bade Shrestha, Karim GA, Wierzba I, Examination of operational limits in gas fueled spark ignition engines, *SAE*, Paper No. 2000-01-1944-SP-1549.

[12] Das LM, Exhaust emission characterization of hydrogen operated engine system, *Int. J. Hydrogen Energy*, 15:833, 1990.

[13] Shioji M, Inoue N, Performance and NO_x formation in a hydrogen premixed charge engine, *Proceedings of 12th World Hydrogen Conference*, Buenos Aires, Argentina, 1469–78, 1998.

[14] Shioji M, Ishayama T, Feasibility of the high-speed hydrogen engine, *International Symposium on Hydrogen Energy*, Osaka, Japan, 1–9, January 2002.

[15] Sierens R, Rosseel E, Backfire mechanism in a carburetted hydrogen fuelled compression ignition engine, *Proceedings of the 12th World Hydrogen Conference*, Buenos Aires, Argentina, 341–53, 1998.

[16] Karim GA, Klat SR, The knock and autoignition characteristics of some gaseous fuels and their mixtures, *J. Inst. Fuel*, 39:109–19, 1966.

[17] Hord J, Is hydrogen a safe fuel?, *Int. J. Hydrogen Energy*, 3:157–176, 1978.

[18] http://www.daimlerchrysler.com.

[19] Leung, WB, et al, *Phys. Lett. A*, 56:425, 1976.

[20] Weast RC, *Handbook of Chemistry and Physics*, 57th ed., CRC Press, 1976.

[21] Schlapbach L, *Hydrogen in Intermetallic Compounds II*, Springer, Heidelberg, 219, 1988.

[22] Huston EL, A liquid and solid storage of hydrogen, *Proceedings of the* 5th *World Hydrogen Energy Conference*, Veziroqlu, T. N., Taylor JB (ed.), Pergamon Press, Oxford, 3, 1984.

[23] Flynn TM, A liquification of gases, *McGraw-Hill Encyclopedia of Science & Technology*, 7th ed., Parker SP (ed.), McGraw-Hill, New York, 10:106, 1992.

[24] Gary Chen and Samim Anghaie based on NASA/NIST databases, http://www.inspi.ufl.edu/data/h_prop_package.html

[25] von Ardenne M, et al, *Effekte der Physik*, Verlag Harri Deutsch, Frankfurt am Main, 712, 1990.

[26] Steinfeld A, *Int. J. Hydrogen Energy*, 27:611, 2002.

[27] Dillon AC, Jones KM, Bekkedahl TA, Kiang CH, Bethune DS, Heben MJ, *Nature*, 386:377–379, 1997.

[28] Christmann K, Hydrogen adsorption on metal surfaces, *Atomistics of Fracture Conference Proceedings*, Latanision and Pickensr (eds.), Plenum, New York, 1981.

[29] Pearson GR, *Chem. Rev.*, 85:41, 1985.

[30] Mueller WM, et al (eds.), *Metal Hydrides*, Academic Press, New York, 1968.

[31] Lennard-Jones JE, *Trans. Faraday Soc.*, 28:333, 1932.

[32] Fukai Y, *Z, Phys. Chem.*, 164:165, 1989.

[33] Switendick AC, *Z. Phys. Chem. N. F.*, 117:89, 1979.

[34] Westlake DJ, *J. Less-Common Met.*, 91:275, 1983.

[35] Rittmeyer P, Wietelmann U, Hydrides, *Ullmann's Encyclopedia of Industrial Chemistry*, 5th ed., Bohnet M, et al (eds.), Wiley-VCH, A13:199, 1996.

[36] Miedema AR, *J. Less-Common Met.*, 32:117, 1973.

[37] Van Mal HH, et al, *J. Less-Common Met.*, 35:65, 1974.

[38] Griessen R, Riesterer T, Heat of formation models, *Hydrogen in Intermetallic Compounds I*, Schlapbach L (ed.), Springer, 219, 1988.
[39] Yvon K, *Chimia*, 52:613, 1998.
[40] Amendola SC, et al, Process For Synthesizing Borohydride Compounds, US Patent, 6 524 542, 2003.
[41] Bogdanovic B, Schwickardi M, *J. Alloys Compd.*, 253–254:1, 1997.
[42] Bogdanovic B, et al, *J. Alloys Compd.*, 302:36, 2000.
[43] Dymova TN, et al, *Dok. Akad. Nauk USSR*, 215:1369, 1974.
[44] Züttel A, et al, *J. Power Sources*, 118:1, 2003.
[45] Schrauzer GN, *Naturwissenschaften*, 42:438, 1955.
[46] Lippard SJ, Ucko DA, *Inorg. Chem.*, 7:1051, 1968.
[47] Lipscomb WN, *Boron Hydrides*, W. A. Benjamin, New York, 1963.
[48] Sandrock G, Thomas G, *Appl. Phys. A*, (2001) 72:153, 2001.
[49] Fichtner M, Fuhr O, *J. Alloys Compd.*, 345:286, 2002.
[50] Fichtner M, et al, *J. Alloys Compd.*, 2003.
[51] Jensen CM, et al, *Int. J. Hydrogen Energy*, 24:461, 1999.
[52] Zidan R, et al, *J. Alloys Compd.*, 285:119, 1999.
[53] Wang J, et al, *Adsorption Science and Technology*, Lee CH, (ed.), World Scientific, Korea, 2003.
[54] Sun D, et al, *J. Alloys Compd.*, 337:L8, 2002.
[55] Gross KJ, et al, *J. Alloys Compd.*, 297:270, 2000.
[56] Jensen C, Gross K, *Appl. Phys. A*, 72:213, 2001.
[57] Thomas G, et al, *J. Alloys Compd.*, 330–332:702, 2002.
[58] Gross KJ, et al, *J. Alloys Compd.*, 330–332:683, 2002.
[59] Gross K, et al, *J. Alloys Compd.*, 330–332:691, 2002.
[60] Chen J, et al, *J. Phys. Chem. B*, 105:11214, 2001.
[61] Ritter JA, Ebner AD, Wang J, Zidan R, *Materials Today*, 6(9):18, 2003.
[62] Reilly JJ, Applications of metal hydrides, *Hydrides For Energy Storage*, Andersen AF, Maeland AJ (eds.), Pregamon Press, 1978.
[63] Lynch FE, Snape E, The role of metal hydrides in hydrogen storage and utilization, *Proc. 2nd World Hydrogen Energy Conf.*, Zurich, 1978, Pregmon Press, Oxford, 3:1475, 1978.
[64] Iijima S, *Nature*, 354:56–58, 1991.
[65] Hamada N, Sawada S, Oshiyama A, *Phys. Rev. Lett.*, 68:54, 1992.
[66] Dresselhaus MS, Dresselhaus G, Eklund PC, *Science Of Fullerenes And Carbon Nanotubes*, Academic Press, New York, 1996.
[67] Cohen ML, *Material Sci. Eng. C*, 15:1–11, 2001.
[68] Darkrim F, Levesque D, Monto Carlo simulation of hydrogen adsorption in single-walled carbon nanotubes, *J. Chem. Phys.*, 109:4981–4984, 1998.
[69] Frackowiak E, Gautier S, Gaucher H, Bonnamy S, Béguin F, Electrochemical storage of lithium in multiwalled carbon nanotubes, *Carbon*, 37:61–69, 1999.

[70] Leroux F, Méténier K, Gautier S, Frackowiak E, Bonnamy S, Béguin F, Electrochemical insertion of lithium in catalytic multi-walled carbon nanotubes, *J. Power Sources*, 81–82:317–322, 1999.

[71] Wu GT, Wang CS, Zhang XB, Yang HS, Qi ZF, He PM, Li WZ, Structure and lithium insertion properties of carbon nanotubes, *J. Electrochem. Soc.*, 146(5):1696–1701, 1999.

[72] Béguin F, Méténier K, Pellenq R, Bonnamy S, Frackowiak E, Lithium insertion in carbon nanotubes, *Mol. Cryst. Liq. Cryst.*, 340:547–552, 2000.

[73] Gao B, Bower C, Lorentzen JD, Fleming L, Kleinhammes A, Tang XP, McNeil LE, Wu Y, Zhou O, Enhanced saturation lithium composition in ball-milled single-walled carbon nanotubes, *Chem. Phys. Lett.*, 327:69–75, 2000.

[74] Claye AS, Fischer JE, Huffman CB, Rinzler AG, Smalley RE, Solid-state electrochemistry of the single wall carbon nanotube system, *J. Electrochem. Soc.*, 147(8):2845–2852, 2000.

[75] Niu C, Sichel EK, Hoch R, Moy D, Tennet H, High power electrochemical capacitors based on carbon nanotube electrodes, *Appl. Phys. Lett.*, 70:1480–1482, 1997.

[76] Frackowiak E, Méténier K, Bertagna V, Béguin F, Supercapacitor electrodes from multiwalled carbon nanotubes, *Appl. Phys. Lett.*, 77:2421–2423, 2000.

[77] Frackowiak E, Béguin F, Carbon materials for the electrochemical storage of energy in capacitors, *Carbon*, 39:937–950, 2001.

[78] Frackowiak E, Jurewicz K, Delpeux S, Béguin F, Nanotubular materials for supercapacitors, *J. Power Sources*, 97–98:822–825, 2001.

[79] Jurewicz K, Delpeux S, Bertagna V, Béguin F, Frackowiak E, Supercapacitors from nanotubes/polypyrrole composites, *Chem. Phys. Lett.*, 347:36–40, 2001.

[80] Nützenadel C, Zuttel A, Chartouni D, Schlapbach L, Electrochemical storage of hydrogen in nanotube materials, *Electrochem. Solid-State Lett.*, 2(1):30–32, 1999.

[81] Rajalakshmi N, Dhathathreyan KS, Govindaraj A, Satishkumar BC, Electrochemical investigation of single-walled carbon nanotubes for hydrogen storage, *Electrochim. Acta*, 45:4511–4515, 2000.

[82] Che G, Lakshmi BB, Martin CR, Fisher ER, Metal-nanocluster-filled carbon nanotubes: catalytic properties and possible applications in electrochemical energy storage and production, *Langmuir*, 15:750–758, 1999.

[83] Britto PJ, Santhanam KSV, Rubio A, Alonso JA, Ajayan PM, Improved charge transfer at carbon nanotube electrodes, *Adv. Mater.*, 11:154–157, 1999.

[84] Agarwal RK, Noh JS, Schwarz JA, Effect of surface acidity of activated carbon on hydrogen storage, *Carbon*, 25:219–226, 1987.

[85] Gregg SJ, Sing KSW, *Adsorption, Surface Area and Porosity*, Academic Press, London & New York, 1967.

[86] Stan G, Cole M, Hydrogen adsorption in nanotubes, *J. Low Temp. Phys.*, 110:539–544, 1998.

[87] Lee SM, Lee YH, Hydrogen storage in single-walled carbon nanotubes, *Appl. Phys. Lett.*, 76(20):2877–2879, 2000.

[88] Dresselhaus MS, Williams KA, Eklund PC, Hydrogen adsorption in carbon materials, *MRS Bull.*, 24:45–50, 1999.

[89] Hwang JY, Lee SH, Sim KS, Kim JW, Synthesis and hydrogen storage of carbon nanofibers, *Synthetic Metals,* 126(1):81-85, 2002.

[90] Kuznetsova A, Mawhinney DB, Naumenko V, Yates Jr. JH, Liu J, Smalley RE, *Chem. Phys. Lett.*, 321:292, 2000.

[91] Brown SDM, Dresselhaus G, Dresselhaus MS, Reversible hydrogen uptake in carbon-based materials, *Recent Advances In Catalytic Materials - Mater. Res. Soc. Symp. Proc.*, Rodriguez NM, Soled SL, Hrbek J (eds.), Warrendale, PA, 497:157–163, 1998.

[92] Stan G, Cole M, Low coverage adsorption in cylindrical pores, *Surf. Sci.*, 395:280–291, 1998.

[93] Vermesse J, Levesque D, *Mol. Phys.*, 77:837, 1992.

[94] Kaneko K, Cracknell RF, Nicholson D, *Langmuir*, 10:4606, 1994.

[95] Kaneko K, Nicholson D, Quirke N, *Mol. Sim.*, 13:161, 1994.

[96] Gadd GE, Blackford M, Moricca S, *Science*, 277:933, 1997.

[97] Teizer W, Hallock RB, Dujardin E, Ebbesen TW, *Phys. Rev. Lett.*, 84:1844, 2000.

[98] Wang Q, Johnson JK, *J. Phys. Chem.*, 107:5108, 1997.

[99] Williams KA, Eklund PC, Monto Carlo simulation of H_2 physisorption in finite-diameter carbon nanotube ropes, *Chem. Phys. Lett.*, 320:352–358, 2000.

[100] Rzepka M, Zlamp P, de la Casa-lillo MA, Physisorption of hydrogen on microporous carbon and carbon nanotubes, *J. Phys. Chem. B*, 102:10894–10898, 1998.

[101] Wang QY, Johnson JK, Optimization of carbon nanotubes arrays for hydrogen adsorption, *J. Phys. Chem. B*, 103:4809–4813, 1999.

[102] Wang QY, Johnson JK, Molecular simulation of hydrogen adsorption in single-walled carbon naotubes and idealized carbon slit pores, *J. Chem. Phys.*, 110(1):577–586, 1999.

[103] Zuttel A, Sudan P, Mauron Ph, Kiyobayashi T, Emmenegger Ch, Schlapbach L, *Int. J. Hydrogen Energy*, 27:203-212, 2002.

[104] Westlake DJ, *J. Less Common Metals*, 91:1–20, 1983.

[105] Fan YY, Liao B, Liu M, Wei YL, Lu MQ, Cheng HM, Hydrogen uptake in vapor-grown carbon nanofibers, *Carbon*, 37:1649–1652, 1999.

[106] Friedlmeier G, Schaaf M, Groll M, *Z. Phys. Chem. N.F.*, 183:185, 1994.

[107] Ströbel R, Jörissen L, Schliermann T, Trapp V, Schütz W, Bohmhammel K, Wolf G, Garche J, *J. Power Sources*, 84:221, 1999.

[108] Benham MJ, Ross DK, *Z. Phys. Chem. N.F.*, 163:25, 1989.

[109] Mommer N, Hirscher M, Cuevas F, Kronmüller H, *J. Alloys Comp.*, 266:255, 1998.

[110] Arellano JS, Molina LM, Rubio A, Alonso JA, Density functional study of adsorption of molecular hydrogen on graphene layers, *J. Chem. Phys.*, 112(18):814–819, 2000.

[111] Dillon AC, Bekkedahl TA, Jones KM, Heben MJ, *Fullerenes*, 3:716, 1999.

[112] Lamari M, Malbrunot P, *AIChE J.*, 46:632, 2000.

[113] Ye Y, Ahn CC, Witham C, Fultz B, Liu J, Rinzler AG, Colbert D, Smith KA, Smalley RE, Hydrogen adsorption and cohesive energy of single-walled carbon nanotubes, *Appl. Phys. Lett.*, 74(16):2307–2709, 1999.

[114] Liu C, Fan YY, Liu M, Cong HT, Cheng HM, Dresselhaus MS, Hydrogen storage in single-walled carbon nanotubes at room temperature, *Science*, 286:1127–1129. 1999.

[115] Nützenadel Ch, Züttel A, Schlapbach L, Electronic properties of novel materials, *Science And Technology Of Molecular Nanostructures*, Kuzmany H, Fink J, Mehring M, Roth S (eds.), American Institute of Physics, New York, USA, 9:462, 1999.

[116] Nützenadel Ch, Züttel A, Emmenegger Ch, Sudan P, Schlapbach L, Sciences and applications of nanotubes, *Fundamental Materials Research Series*, Thorpe MF (ed.), Kluwer Academic Publishing/Plenum Press, Dordrecht/New York, 10:205.

[117] Dillon AC, Gennet T, Alleman JL, Jones KM, Parilla PA, Heben MJ, Carbon nanotube materials for hydrogen storage, *Proceedings of the 2000 Hydrogen Program Review*, NREL/CP-570-28890.

[118] Hirscher M, Becher M, Haluska M, Detlaff-Weglikowska U, Quintel A, Duesberg GS, Choi Y-M, Downes P, Hulman M, Roth S, Stepanek I, Bernier P, *Appl. Phys. A*, 2001.

[119] Liu C, Cong HT, Li F, Tan PH, Cheng HM, Lu K, Zhou BL, Semi-continuous synthesis of single-walled carbon nanotubes by a hydrogen arc discharge method, *Carbon*, 37:1865–1868, 1999.

[120] Cheng HM, Liu C, Fan YY, Li F, Su G, Cong HT, He LL, Liu M, Synthesis and hydrogen storage of carbon nanofibers and single-walled carbon nanotubes, *Z. Metallkd.*, 91:306–311, 2000.

[121] Yang QH, Fan YY, Li F, Liu C, Liu M, Fan YZ, Cheng HM, Wang MZ, Analysis of pore structure of carbon nanotube, *Extended Abstracts, Eurocarbon 2000*, *Berlin, German*, German Carbon Group (DKG), 1023–1024, 2000.

[122] Darkrim FL, Levesque D, *J. Phys. Chem. B*, 104:6773, 2000.

[123] Cheng HM, Li F, Sun X, Brown SDM, Pimenta MA, Marucci A, Dresselhaus G, Dresselhaus MS, Bulk morphology and diameter distribution of single-walled carbon nanotubes synthesized by catalytic decomposition of hydrocarbon, *Chem. Phys. Lett.*, 289:602–610, 1998.

[124] Zhu HW, Ci LJ, Chen A, Mao ZQ, Xu CL, Xiao X, Wei BQ, Liang J, Wu DH, *Proceedings of the 13th World Hydrogen Energy Conference*, Beijing, China, Mao ZQ, Veziroglu TN (eds.), International Hydrogen Association, 560, 2000.

[125] Wu HB, Chen P, Lin J, Tan KL, *Int. J. Hydrogen Energy*, 25:261, 2000.

[126] Chen P, Wu X, Lin J, Tan KL, High H_2 uptake by alkali-doped carbon nanotubes under ambient pressure and moderate temperatures, *Science*, 285:91–93, 1999.

[127] Yang RT, Hydrogen storage by alkali-doped carbon naotubes-revisited, *Carbon*, 38:623–626, 2000.

[128] Pinkerton F, Wickle B, Olk C, Tibbetts G, Meisner G, Meyer MS, Herbst J, *Proceedings of the 10th Canadian Hydrogen Conference*, Quebec, Canadian Hydrogen Association, 2000.

[129] Chambers A, Park C, Baker RTK, Rodriguez NM, Hydrogen storage in graphite nanofibers, *J. Phys. Chem. B*, 102:4253–4256, 1998.

[130] Rodriguez N, *Proceedings of the Ninth Canadian Hydrogen Conference 'Hydrogen Power Now'*, Vancouver, Canada, Howard PF (ed.), Canadian Hydrogen Association, 1999.

[131] Park C, Anderson PE, Chambers A, Tan CD, Hidalgo R, Rodriguez NM, Further studies of the interaction of hydrogen with graphite nanofibers, *J. Phys. Chem. B*, 103:10572–10581, 1999.

[132] Browning DJ, Gerrard ML, Laakeman JB, Mellor IM, Mortimer RJ, Turpin MC, *Proceedings of the 13th World Hydrogen Energy Conference*, Beijing, China, Mao ZQ, Veziroglu TN (eds.), International Hydrogen Association, 580, 2000.

[133] Gupta BK, Awasthi K, Srivastava ON, *Proceedings of the 13th World Hydrogen Energy Conference*, Beijing, China, Mao ZQ, Veziroglu TN (eds.), International Hydrogen Association, 487, 2000.

[134] Orimo S, Majer G, Fukunaga T, Züttel A, Schlapbach L, Fujii H, *Appl. Phys. Lett.*, 75:3093–3095, 1999.

[135] Darkrim FL, Malbrunot P, Tartaglia GP, *Int. J. Hydrogen Energy*, 27:193-202, 2002.

[136] Hirscher M, Becher M, Haluska M, von Zeppelin F, Chen X, Weglikowska UD, Roth S, *J. Alloys Comp.*, 356-357:433-437, 2003.

[137] Hirscher M, Becher M, Haluska M, Quintel A, Skakalova V, Choi YM, Dettlaff-Weglikowska U, Roth S, Stepanek I, Bernier P, Leonhardt A, Fink J, Hydrogen storage in carbon nanostructures, *MH2000, Noosa, Australia*, J. Alloys Compounds, 2001.

[138] Hirscher M, Becher M, Quintel A, Skakalova V, Choi YM, Roth S, Stepanek I, Bernier P, Leonhardt A, Fink J, Hydrogen desorption measurements on carbon nanotubes and graphite, *Extended Abstracts, Eurocarbon 2000, Berlin, German,* German Carbon Group (DKG), 91–92, 2000.

[139] Beguin F, Frackpwiak E, Storage of energy in carbon nanotubes, *Extended Abstracts, Eurocarbon 2000, Berlin, German,* German Carbon Group (DKG), 9–10, 2000.

[140] Orimo S, Majer G, Fukunaga T, Züttel A, Schlapbach L, Fujii H, Hydrogen in the mechanically prepared nanostructured graphite, *Extended Abstracts, Eurocarbon 2000, Berlin, German,* German Carbon Group (DKG), 85–86, 2000.

[141] Nützenadel C, Züttel A, Emmenegger C, Sudan P, Schlapbach L, Electrochemical storage of hydrogen in carbon single wall nanotubes, *Science and Application of Nanotubes*, Tománek D, Enbody RJ (eds.), Kluwer Academic Publishing/Plenum Press, New York, 205–213, 2000.

[142] Yin YF, Mays T, McEnamey B, *Langmuir*, 103:10521, 2000.

[143] Bandow S, Rao AM, Williams KA, Thess A, Smalley RE, Eklund PC, *J. Phys. Chem. B*, 102:429, 1998.

[144] Stepanek I, de Menorval LC, Edwards R, Bernier P, *AIP Conf.*, 486:456, 1999.

[145] Stepanek I, Maurin G, Bernier P, Gavillet J, Loiseau A, Edwards R, *Chem. Phys. Lett.*, 331:125, 2000.

[146] Basca R, Laurent C, Peigney A, Basca W, Vaugien T, Rousset A, *Chem. Phys. Lett.*, 323:526, 2000.

[147] Hiura H, Ebbesen TW, Tanigaki K, *Adv. Mater.*, 7:2726, 1995.

[148] Ajayan PM, Ebbesen TW, Ichihashi T, Iijima S, Tanigaki K, Hiura H, *Nature*, 362:522, 1993.

[149] Orimo S, Majer G, Fukunaga T, Zutel A, Schlapbach L, Fujii H, *Appl. Phys. Lett.*, 75:20, 1999.
[150] Lagrange P, Herold A, *Carbon*, 16:235, 1987.
[151] Darkrim F, Malbrunot P, *Proceedings of the 12th World Hydrogen Energy Conference, Buenos Aires, Argentina*, Bolchich JC, Veziroglu TN (eds.), International Hydrogen Association, 1201, 1998.
[152] Viswanathan B, *Bull. Catal. Soc. India*, 11(1), 2001.